410197

WT-914 (EX)
EXTRACTED VERSION

OPERATION CASTLE

Project 2.3
Neutron Flux Measurements

March-May 1954

Headquarters Field Command
Armed Forces Special Weapons Project
Sandia Base, Albuquerque, New Mexico

October 1955

NOTICE

This is an extract of WT-914, Operation CASTLE, which remains classified SECRET/RESTRICTED DATA as of this date.

Extract version prepared for:

Director
DEFENSE NUCLEAR AGENCY
Washington, D.C. 20305

1 April 1981

Approved for public release; distribution unlimited.

REPORT DOCUMENTATION PAGE

READ INSTRUCTIONS BEFORE COMPLETING FORM

1. REPORT NUMBER: WT-914 (EX)
2. GOVT ACCESSION NO.:
3. RECIPIENT'S CATALOG NUMBER:
4. TITLE (and Subtitle): Operation CASTLE - Project 2.3 Neutron Flux Measurements
5. TYPE OF REPORT & PERIOD COVERED:
6. PERFORMING ORG. REPORT NUMBER: WT-914 (EX)
7. AUTHOR(s): T. D. Hanscome, D. K. Willett, A. Brodsky
8. CONTRACT OR GRANT NUMBER(s):
9. PERFORMING ORGANIZATION NAME AND ADDRESS: Headquarters Field Command, Armed Forces Special Weapons Project, Sandia Base, Albuquerque, N.M.
10. PROGRAM ELEMENT, PROJECT, TASK AREA & WORK UNIT NUMBERS:
11. CONTROLLING OFFICE NAME AND ADDRESS:
12. REPORT DATE: October 1955
13. NUMBER OF PAGES: 79
14. MONITORING AGENCY NAME & ADDRESS (if different from Controlling Office):
15. SECURITY CLASS. (of this report): Unclassified
15a. DECLASSIFICATION/DOWNGRADING SCHEDULE:
16. DISTRIBUTION STATEMENT (of this Report): Approved for public release; unlimited distribution.
17. DISTRIBUTION STATEMENT (of the abstract entered in Block 20, if different from Report):
18. SUPPLEMENTARY NOTES: This report has had the classified information removed and has been republished in unclassified form for public release. This work was performed by Kaman Tempo under contract DNA001-79-C-0455 with the close cooperation of the Classification Management Division of the Defense Nuclear Agency.
19. KEY WORDS (Continue on reverse side if necessary and identify by block number):
Operation CASTLE
Neutron Flux Measurements
Instrumentation
Neutron Fission Detectors
Neutron Measurements
Gamma Rays
Experiment Design
20. ABSTRACT (Continue on reverse side if necessary and identify by block number):

FOREWORD

This report has had classified material removed in order to make the information available on an unclassified, open publication basis, to any interested parties. This effort to declassify this report has been accomplished specifically to support the Department of Defense Nuclear Test Personnel Review (NTPR) Program. The objective is to facilitate studies of the low levels of radiation received by some individuals during the atmospheric nuclear test program by making as much information as possible available to all interested parties.

The material which has been deleted is all currently classified as Restricted Data or Formerly Restricted Data under the provision of the Atomic Energy Act of 1954, (as amended) or is National Security Information.

This report has been reproduced directly from available copies of the original material. The locations from which material has been deleted is generally obvious by the spacings and "holes" in the text. Thus the context of the material deleted is identified to assist the reader in the determination of whether the deleted information is germane to his study.

It is the belief of the individuals who have participated in preparing this report by deleting the classified material and of the Defense Nuclear Agency that the report accurately portrays the contents of the original and that the deleted material is of little or no significance to studies into the amounts or types of radiation received by any individuals during the atmospheric nuclear test program.

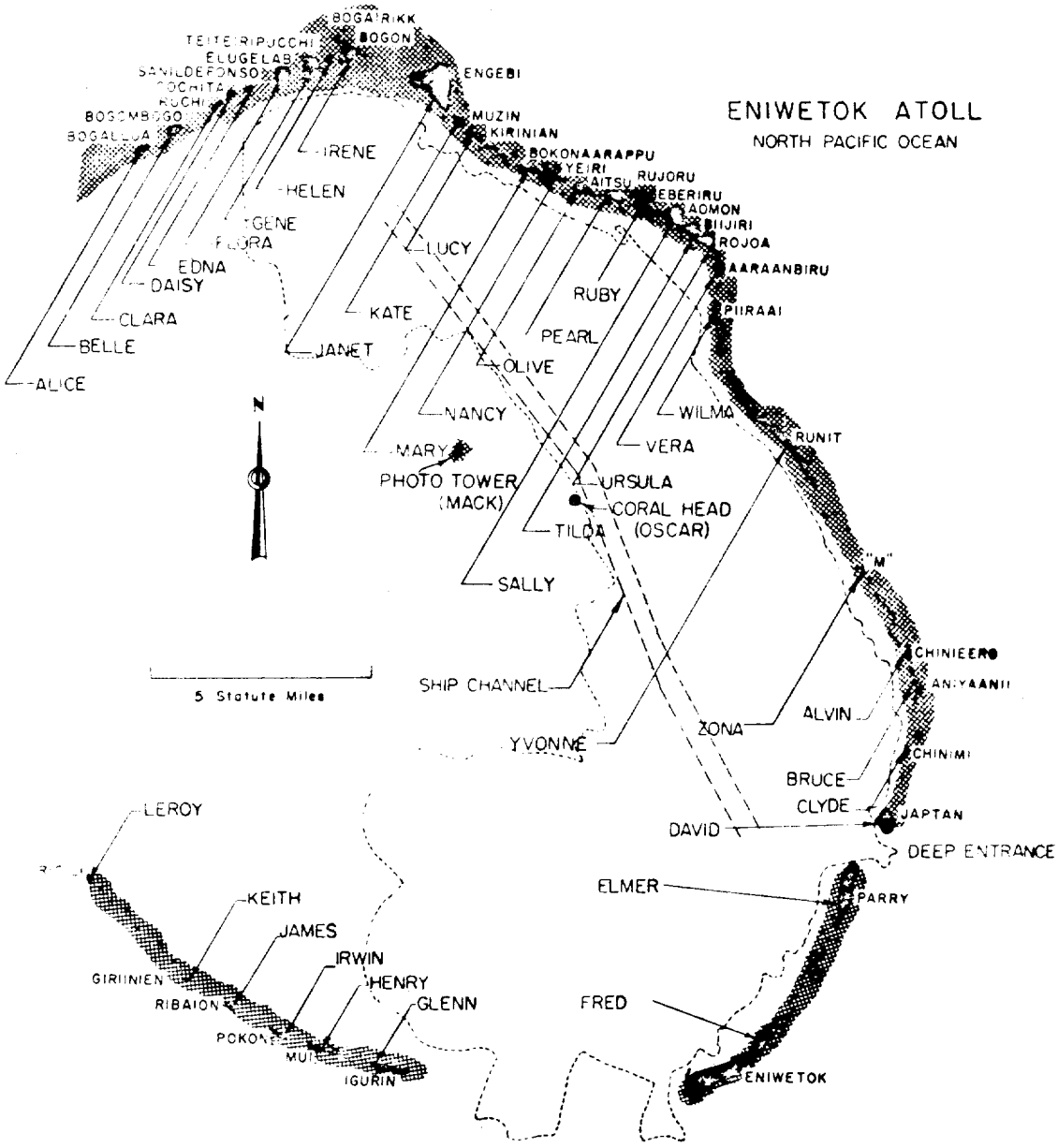
ENIWETOK ATOLL
NORTH PACIFIC OCEAN
BOGA
BOGON
ENGEBI
MUZIN
KIRINIAN
BOKONAARAPPU
YEIRI
AITSU
RUJORU
EBERIRU
AOMON
IIJIRI
ROJOA
AARAANBIRU
PIIRAAI
IRENE
HELEN
LUCY
RUBY
KATE
PEARL
OLIVE
EDNA
DAISY
CLARA
BELLE
ALICE
JANET
NANCY
WILMA
MARY
VERA
RUNIT
PHOTO TOWER
(MACK)
URSULA
CORAL HEAD
(OSCAR)
TILOA
SALLY
"M"
CHINIEERO
ANIYAANII
5 Statute Miles
SHIP CHANNEL
YVONNE
ZONA
ALVIN
CHINIMI
BRUCE
CLYDE
JAPTAN
DAVID
DEEP ENTRANCE
ELMER
PARRY
LEROY
KEITH
JAMES
IRWIN
HENRY
GLENN
FRED
ENIWETOK

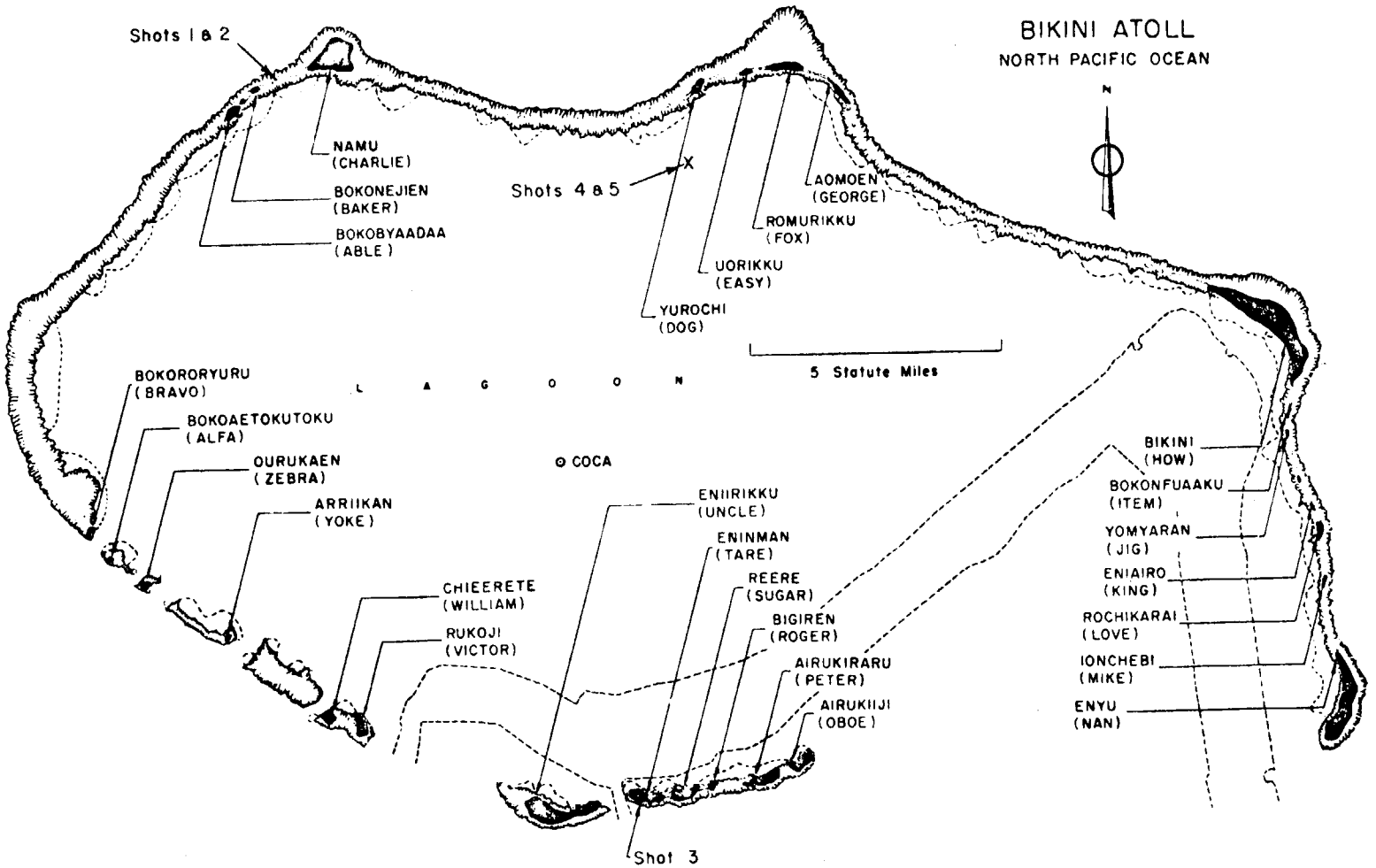
BIKINI ATOLL
NORTH PACIFIC OCEAN
N
Shots 1 & 2
Shots 4 & 5
Shot 3
NAMU (CHARLIE)
BOKONEJIEN (BAKER)
BOKOBYAADAA (ABLE)
AOMOEN (GEORGE)
ROMURIKKU (FOX)
UORIKKU (EASY)
YUROCHI (DOG)
5 Statute Miles
L A G O O N
BOKORORYURU (BRAVO)
BOKOAETOKUTOKU (ALFA)
OURUKAEN (ZEBRA)
ARRIIKAN (YOKE)
CHIEERETE (WILLIAM)
RUKOJI (VICTOR)
COCA
ENIIRIKKU (UNCLE)
ENINMAN (TARE)
REERE (SUGAR)
BIGIREN (ROGER)
AIRUKIRARU (PETER)
AIRUKIIJI (OBOE)
BIKINI (HOW)
BOKONFUAAKU (ITEM)
YOMYARAN (JIG)
ENIAIRO (KING)
ROCHIKARAI (LOVE)
IONCHEBI (MIKE)
ENYU (NAN)

GENERAL SHOT INFORMATION

	Shot 1	Shot 2	Shot 3	Shot 4	Shot 5	Shot 6
DATE	1 March	27 March	7 April	26 April	5 May	14 May
CODE NAME (Unclassified)	Bravo	Romeo	Koon	Union	Yankee	Nectar
TIME*	06:40	06:25	06:15	06:05	06:05	06:15
LOCATION	Bikini, West of Charlie (Namu) on Reef	Bikini, Shot 1 Crater	Bikini, Tare (Eninman)	Bikini, on Barge at Intersection of Arcs with Radii of 6900' from Dog (Yurochi) and 3 Statute Miles from Fox (Aomoen).		Eniwetok, IVY Mike Crater, Flora (Elugelab)
TYPE	Land	Barge	Land	Barge	Barge	Barge
HOLMES & NARVER COORDINATES	N 170,617.17 E 76,163.98	N 170,635.05 E 75,950.46	N 100,154.50 E 109,799.00	N 161,698.83 E 116,800.27	N 161,424.43 E 116,688,15	N 147,750.00 E 67,790.00

* APPROXIMATE

ABSTRACT

Project 2.3 was assigned the problem of measuring the neutron flux encountered in the detonation of the nuclear devices at Operation CASTLE. The techniques used to accomplish this task are the same as those used at Operations SNAPPER and UPSHOT-KNOTHOLE. Gold, sulfur, and tantalum were used to measure the flux in the thermal region and the region above 3 Mev. The fission detectors were used to measure the 1 Mev region of the neutron spectrum and to give an idea of the shape of the spectrum above that point.

Because of the short half lives of some of the induced activities it was necessary to provide counting facilities in the field. Two trailers were installed on Elmer for this purpose. These two units were equipped to handle the counting of gold and plutonium. The remaining samples were sent to Naval Research Laboratory for counting.

The plutonium samples were included to provide data in the region above 200 ev. Oak Ridge National Laboratory supplied these samples and the personnel to handle them.

Due to the unanticipated situation which arose after the firing of Shot 1 and the long delays which followed, the participation of Project 2.3 was considerably modified. This group exposed samples on only the first two shots. Because of shifts in shot sites and the modification of the Shot 5 weapon it was deemed advisable to curtail further participation.

The data acquired in the Shots 1 and 2 indicate that the neutron flux is relatively small outside the radius of extreme damage caused by blast and thermal radiation.

PAGE 6

OF DOCUMENT 410 197

WAS NOT PROVIDED

FOREWORD

This report is one of the reports presenting the results of the 34 projects participating in the Military Effects Tests Program of Operation CASTLE, which included six test detonations. For readers interested in other pertinent test information, reference is made to WT-934, Summary of Weapons Effects Tests, Military Effects Program. This summary report includes the following information of possible general interest.

a. An over-all description of each detonation, including yield, height of burst, ground zero location, time of detonation, ambient atmospheric conditions at detonation, etc., for the six shots.
b. Discussion of all project results.
c. A summary of each project, including objectives and results.
d. A complete listing of all reports covering the Military Effects Tests Program.

ACKNOWLEDGEMENTS

We wish to extend our thanks to the Oak Ridge National Laboratory for the help given us by M. Slater and P. N. Hensley, without whose able assistance the work on plutonium could not have been included in this project. Our thanks also to G. S. Hurst of the same facility for his aid and cooperation.

We wish to acknowledge here the help of B. Cassen of University of California, Los Angeles, who lent some of his germanium detectors for exposure in this series of tests and gave us the opportunity of furthering the development of this neutron detection technique.

The authors would also like to acknowledge the work of V. H. Byrd and the field crew under his supervision. The work of Mr. Byrd and his crew was vital to the successful completion of the project.

Mr. W. Biggers and the 14.1 crew from Los Alamos Scientific Laboratory are also to be thanked for the assistance they gave this project, in the use of their samples and instrument line and the aid rendered in the recovery operations.

In our attempts to obtain improvement in germanium crustals, we have had the cooperation and advice of Dr. M. Becker of the Semi-Conductor Division of Hughes Aircraft.

PAGE 8

OF DOCUMENT 410197

WAS NOT PROVIDED

CONTENTS

ILLUSTRATIONS

TABLES

CHAPTER 1

OBJECTIVES

1.1 OBJECTIVES

It was the purpose of this project to provide data on the neutron fluxes present in the detonation of the nuclear devices in Operation CASTLE. This work provides information for the evaluation of the effects on equipment, materials, and personnel exposed to the radiations of such devices.

In the light of recent findings, that the maximum biological effect results from neutrons concentrated in the region of 1 Mev, it was deemed advisable to make a more thorough investigation of this region of the neutron spectrum. Plutonium was used in the CASTLE series for this purpose.

In addition to the support rendered the biomedical people, a second objective of the project was to provide data on how the radiation of larger [redacted] devices compared both as to intensity and spectrum, with the smaller, more standard weapons studied in previous tests.

Another objective of this project was to further the development of new methods of neutron dosimetry. For this purpose germanium crystal dosimeters were placed in the field with the cooperation of the Medical Physics Section of University of California at Los Angeles. This afforded an opportunity to test new and more sensitive germanium detectors.

PART I

THRESHOLD FISSION DETECTORS

CHAPTER 2

EXPERIMENT DESIGN

2.1 INTRODUCTION

The methods used to make the neutron measurements were similar to those used in Operations SNAPPER and UPSHOT-KNOTHOLE[1,2] The general technique is that of neutron activation of various elements, that is, a sample of a given element is exposed to a neutron flux which induces an amount of activity proportional to that flux. Under ideal conditions a single activity is induced in the sample by neutrons of a discrete energy, thus the activity becomes a measure of the number neutrons of that energy which passed through the sample. Practically, it is not quite so simple however, for few, if any, elements respond so nicely. Most samples used respond to neutrons above a certain energy or, as in the case of gold, below a certain energy. Gold is used to detect thermal neutrons since its capture cross section rises sharply below about 1 ev, the resulting activity has a characteristic half life of 64.4 hours. It can be seen from the foregoing that a number of different elements must be used to cover the anticipated neutron spectrum since any given sample will yield information about only one energy in that spectrum. Project 2.3 used a number of different samples, each of which will be treated separately in succeeding paragraphs.

Since the activity at the instant following exposure to neutrons is the activity of interest, all counting rates must be extrapolated back to time T_o, the time of exposure. Hence the initial count rate becomes the measure of the neutron flux and all count rate data taken on the exposed samples is treated in such a manner as to yield this information.

2.1.1 Detectors

2.1.1.1 Gold

Gold is used as a thermal neutron detector. It has a relatively long history in the field of neutron detection in connection with weapons effects tests, having been used at RANGER[3] and GREENHOUSE[4] as well as at SNAPPER and UPSHOT-KNOTHOLE. Thermal neutrons cause an (n,γ) reaction which results in Au^{198}. The Au^{198} decays by the emission of a 0.97 Mev beta ray and an 0.41 gamma ray in cascade to stable Hg^{198}.

Dual gold samples must be used because of a resonance in the gold cross section at about 3-5 ev (Fig. 2.1.) One sample is cadmium shielded, the cadmium absorbing all thermal neutrons and passing those neutrons above its "cutoff" (1 ev). By taking a difference between the unshielded and the shielded samples the effect of the gold resonance is eliminated, this so called "cadmium difference" is then the measure of the thermal neutron flux.

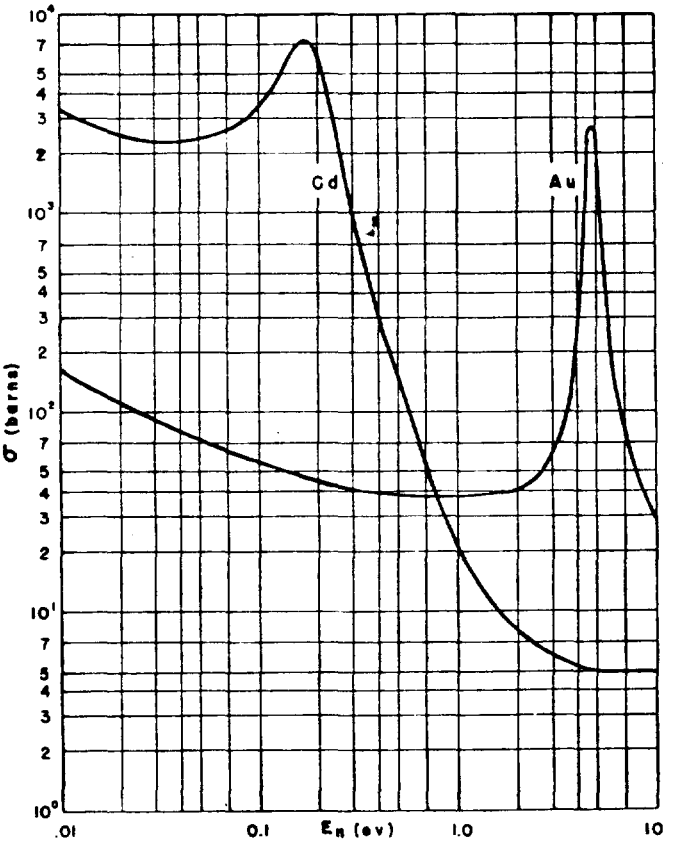

Fig. 2.1 Gold and Cadmium Cross Sections

2.1.1.2 Tantalum

Because of the relatively high cross section of gold for the (n,γ) reaction, the gold samples tend to become too active to count for some time after exposure when irradiated in high thermal fluxes. This leads to prohibitive counting losses or long time delays. To get around this difficulty tantalum is used as an auxiliary thermal detector, since its cross section is only 0.003 that of gold it can be exposed to much higher fluxes without leading to excessively high counting rates. The tantalum samples are subject also to an (n,γ) reaction under thermal neutron bombardment, this reaction leads to the 117 day activity of Ta^{182} There is also the possibility of a 16.4 min. activity appearing from the (n,γ) reaction and an 8.0 hr activity from a (γ,n) and the (n,2n) reactions resulting in Ta^{180}. Fortunately a combination of small cross section and short half life renders the 16.4 min activity no problem. This group has never detected the presence of any 8.0 hr activity.

Because of the presence of several resonances in the tantalum cross section curve it is necessary to make use of the cadmium difference technique in this instance also.

2.1.1.3 Sulfur

Sulfur has a resonance in the region of 2 Mev, the fact that this resonance occurs just above the point where the reaction cross section starts to rise on a barrier penetration curve produces, in effect, a threshold. The effective threshold for the $S^{32}(n,p)P^{32}$ reaction is taken to be 3 Mev and it is assumed that the cross section remains flat above that point. Sulfur then responds to all neutrons above 3 Mev.

The (n,p) reaction results in P^{32} which decays by beta emission with a 14.59 day half life.

Sulfur samples were exposed in powder form in steel containers. (Fig. 2.2). When being prepared for counting, the samples of relatively high counting rate were pressed into 1 in. pellets 1/8 in. thick and counted on an end window counter. Those samples which had low activity were melted at 130°C. and poured into a cylindrical mold (Fig. 2.3). The resulting sample was a 1/8 in. thick sulfur cylinder inside a brass sleeve. This cylinder was slipped over a thin walled aluminum counter tube, the counter tube was hooked in anti-coincidence with a shielding ring of nine similar tubes to lower the background counting rate. With this system it is possible to detect total fluxes as low as 10^6 neuts/cm^2.

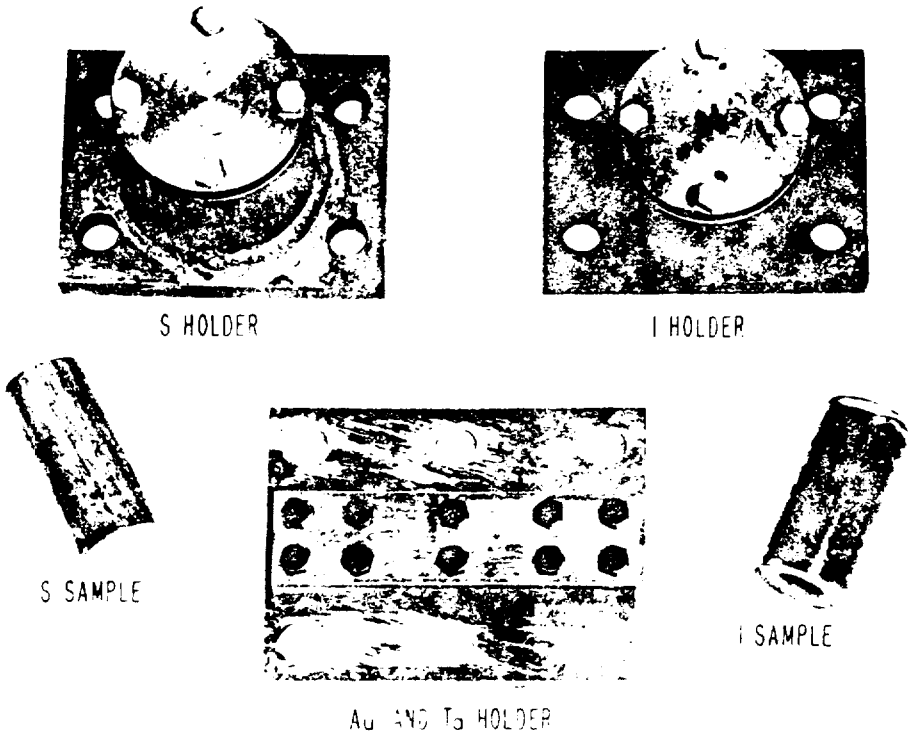

Fig. 2.2 Sample Exposure Containers

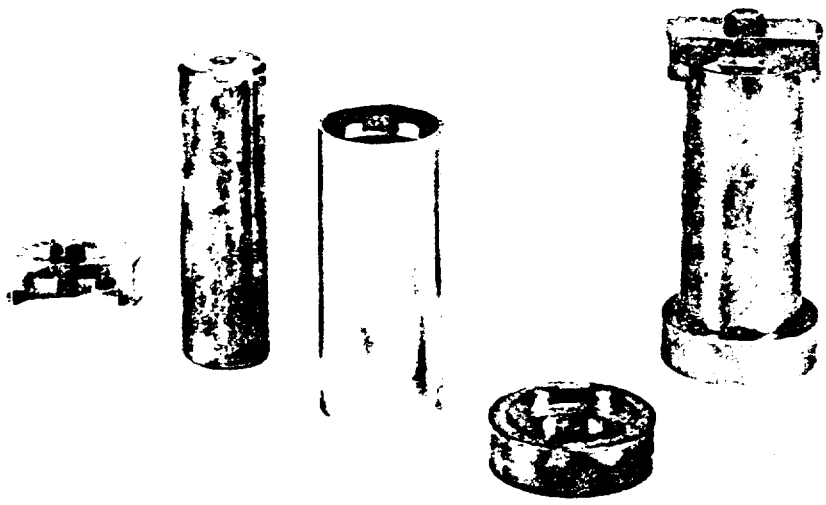

Fig. 2.3 Sulfur Mold

2.1.1.4 Iodine

Iodine has a threshold for the (n,2n) reaction at 9.3 Mev. Being monoisotopic iodine makes a convenient detector. The reaction of interest is I^{127} (n,2n) I^{126}, the half life of the product I^{126} is 13 days. A complication arises from the fact that I^{127} is subject, also, to a (γ,n) reaction. To enable us to differentiate between the results of these two reactions the iodine is exposed in two thicknesses of lead. By this means the effect of the (γ,n) reaction may be subtracted from the desired one. (See Section 2.4.2 for further discussion.) The contribution of neutron reactions within the lead does not seriously enter this correction since any γ induced product in the sample is the result of two reactions. In the first instance the γ ray is the result of an (n,γ) reaction in the lead (or some other reaction) which has a cross section and then the (γ,n) reaction in iodine has a cross section which makes the resultant activity very low in probability with respect to the original (γ,n) reaction.

The exposure container for iodine was a steel container sealed with a copper gasket. The iodine is in pure crystal form when exposed, for counting purposes it is ground slightly in a mortar to break down the larger crystals and poured into a plastic cylinder with a thin inner wall (0.010 in.). (See Fig. 2.4.) This unit is then slipped over the center tube of a counting assembly similar to that used to count the low activity sulfur.

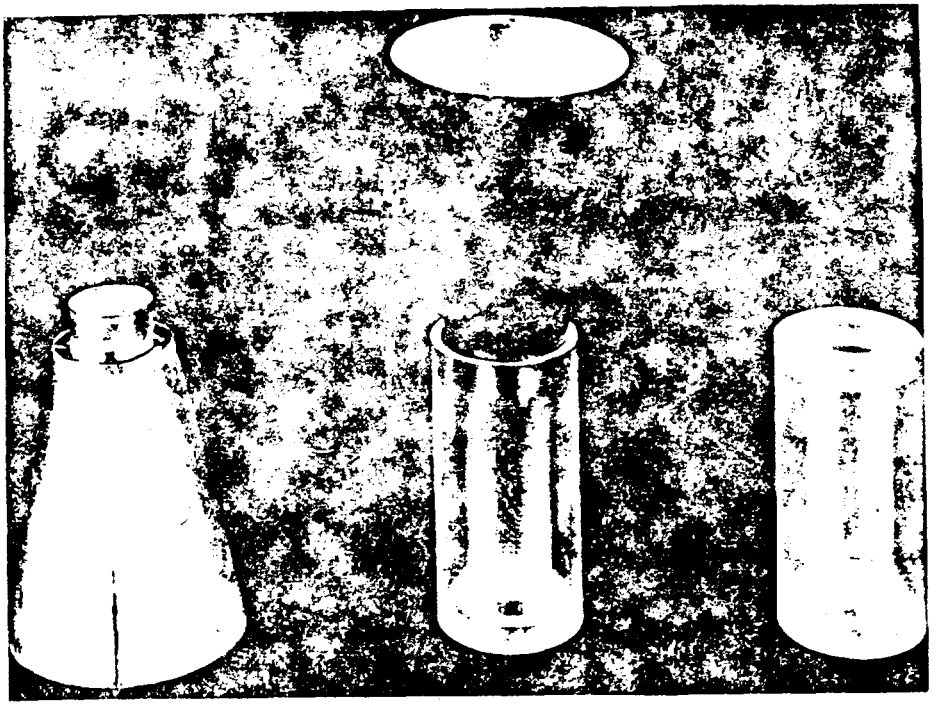

Fig. 2.4 Iodine Sample Holder and Loading Funnel

2.2 FIELD OPERATIONS

2.2.1 Station Design

The field installations used by Project 2.3 were of two distinct types, each of which will be described independently in the following paragraphs. The stations were designed with the idea in mind of keeping the samples outside the "fire-ball" of the weapon, and away from the zone in which great design and construction costs would be required to provide a protection, for the samples, against loss to blast damage.

The "Bunker" type station was essentially a large concrete block anchored to the ground and below the surface of the ground, except for one sloping surface, facing the point of detonation, which protruded about 18 in. A steel panel about 1 in. thick and covering the entire face of the exposed concrete, was bolted to this surface. The samples to be exposed were secured to the steel plate by means of heavy bolts. There were cavities in the concrete, behind the plate, for mounting the shielded iodine samples. This type of sample station was designed by the "J" Division at Los Alamos Scientific Laboratory (LASL), and was used by Project 2.3 in cooperation with them. The "Bunker" type of station was used in the 50-100 psi region at ranges of 2000 to 3000 yd from ground zero.

Recovery from these stations was made either by removing the whole plate from the concrete block or by unfastening the samples

individually from the steel plate, whichever proved simpler at the time of recovery. A complete drawing of this installation is shown in Fig. 2.5.

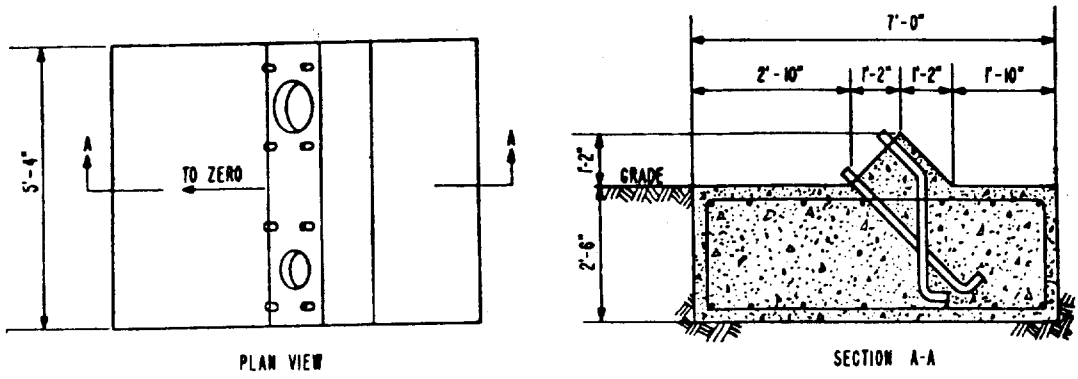

Fig. 2.5 LASL Bunker Station

Fig. 2.6 Sample Mounting Plate

The "Wide Flange" section was the second type of installation to be used by Project 2.3. It was actually a 12 in. H type piling, driven approximately 15 ft into coral with roughly 6 ft above the surface of the water or ground, depending upon the location. A plate 3 ft high by 15 in. wide was bolted to the upper end of the exposed section (Fig. 2.6). It was to this steel plate that the samples were bolted. These sample

stations were designed to provide for installation in either shallow water or on the islands to compensate for the lack of real estate. The "Wide Flange" section was designed to withstand overpressures up to 50 psi and was used at ranges of 3000-5000 yd from ground zero. (See Fig. 2.7.)

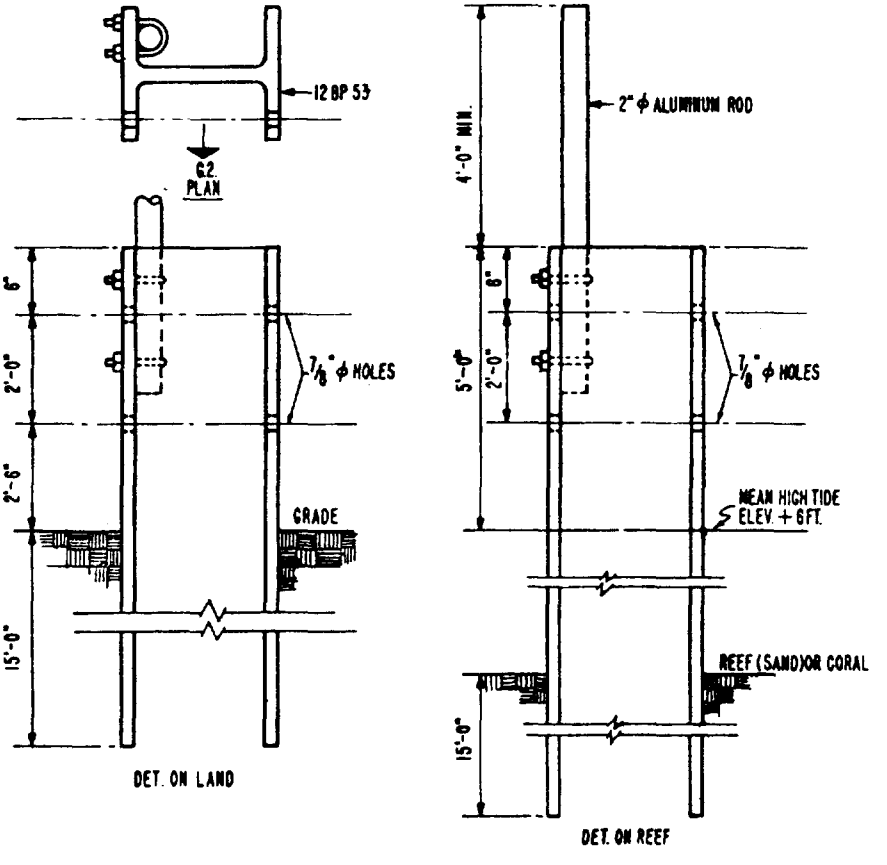

Fig. 2.7 Wide Flange Station

Only one H type piling was used for Shot 1. It was located west of Able on the reef, 2600 yd from the Shot 1 ground zero. This station failed to survive and all samples on it were lost. The remaining piling stations on Fox and George were unused due to the change in shot schedule.

2.2.2 Participation

Project 2.3 participated in the first two shots. Listed in Table 2.1 are the samples which were exposed, the stations at which they were placed, the range and samples which were recovered.

TABLE 2.1 - Project 2.3 Participation

Shot	Station	Range (yd)	Samples	Results
1	231.02	2592	Au,Ta,S,I,Pu, U,Zr,Ge,Np	Destroyed
	1401	2500	Au,Ta,S,I	Recovered
	1403.01	2200	Pu,U,Ge,Np	Damaged but recovered
	1403.02	2100	Au,Ta,S,I,Ge	Recovered
	1403.03	2000	Pu,U,Ge,Np	Recovered
	1403.04	1900	Ge	Recovered
	1403.05	1800	Ge,U,Np	Recovered
	1403.06	1700	Ge	Recovered
2	1401	2500	U,Np	Recovered
	1402	1307	Ge	Recovered
	1403.02	2100	Ge,U,Np	Recovered
	1403.03	2000	Pu,Ge,U,Np,T	Recovered
	1403.04	1900	Pu,Ge,U,Np,T	Lost from lagoon
	1403.05	1800	Pu,Ge,U,Np,T	Recovered later
	1403.06	1700	Pu,Ge,U,Np,T	Partially recovered

Recovery was delayed after both shots, beyond the time originally planned on. On the Shot 1 recovery was not effected until B plus 5 days and on Shot 2 it was not completed until shot day plus 3. As may be noted in that part of this report on the plutonium, the late recovery affected the calibration of the plutonium samples. The recovery operations were carried out as planned by means of helicopter and DUKW with no serious difficulties despite the rather high residual radiation encountered.

Figure 2.8 shows the station locations used by Project 2.3. The eight stations located on the northern run of the atoll were not used due to changes in participation.

2.2.3 Field Counting

For the purposes of counting at the Pacific Proving Grounds two vans were equipped. One was a standard cargo trailer modified for this purpose, the other was an ANMDQ/1, mobile radiochemistry laboratory, which has been slightly modified, loaned to us by the Signal Corps.

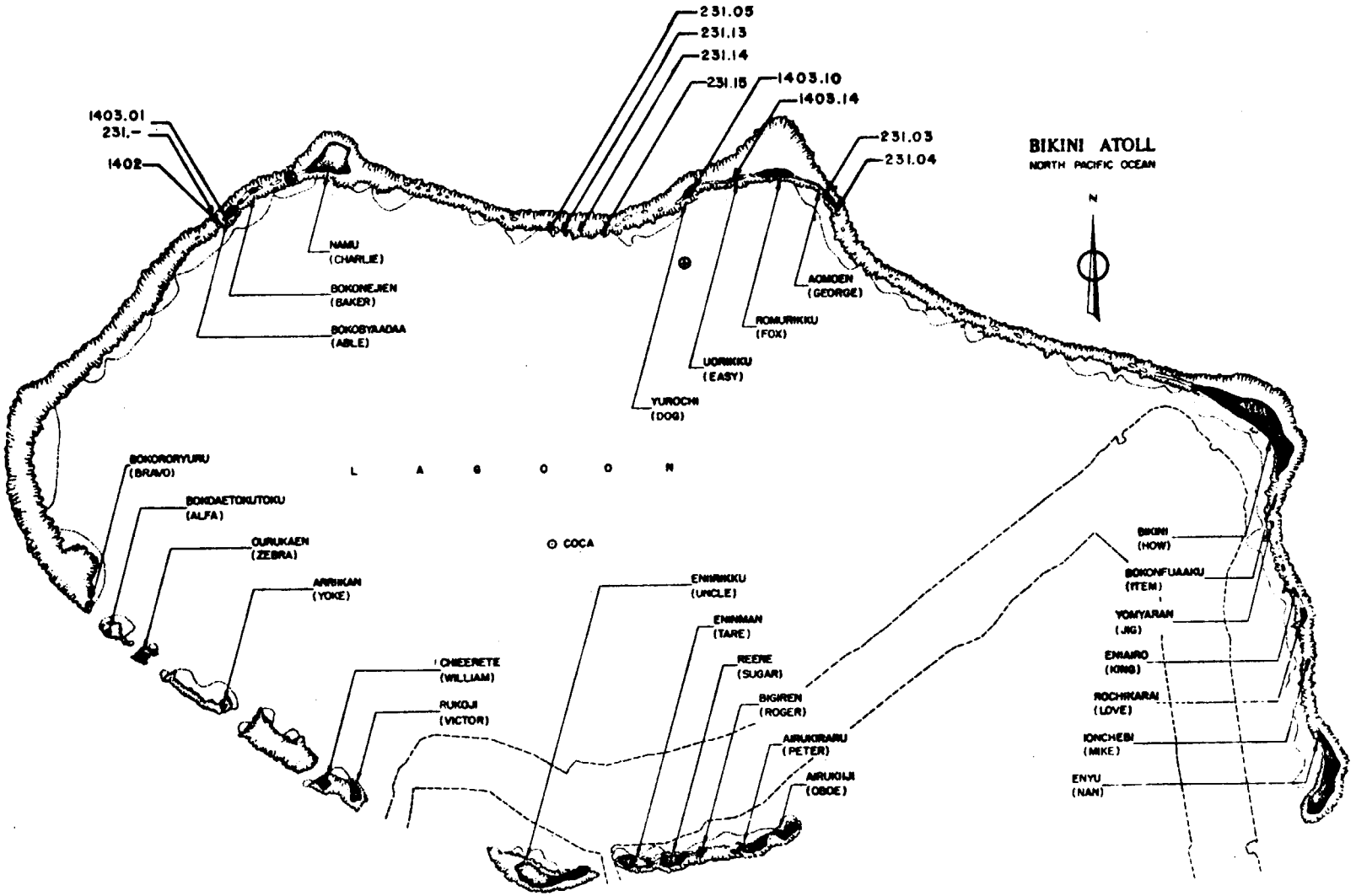

Fig. 2.8 Station Locations

The Naval Research Laboratory (NRL) van was air-conditioned and contained facilities for counting [redacted] plutonium in addition to those for test and repair of electronic components. Provision was made in this trailer for the processing of data and the preparation of report material. (See Figs. 2.9 and 2.10.)

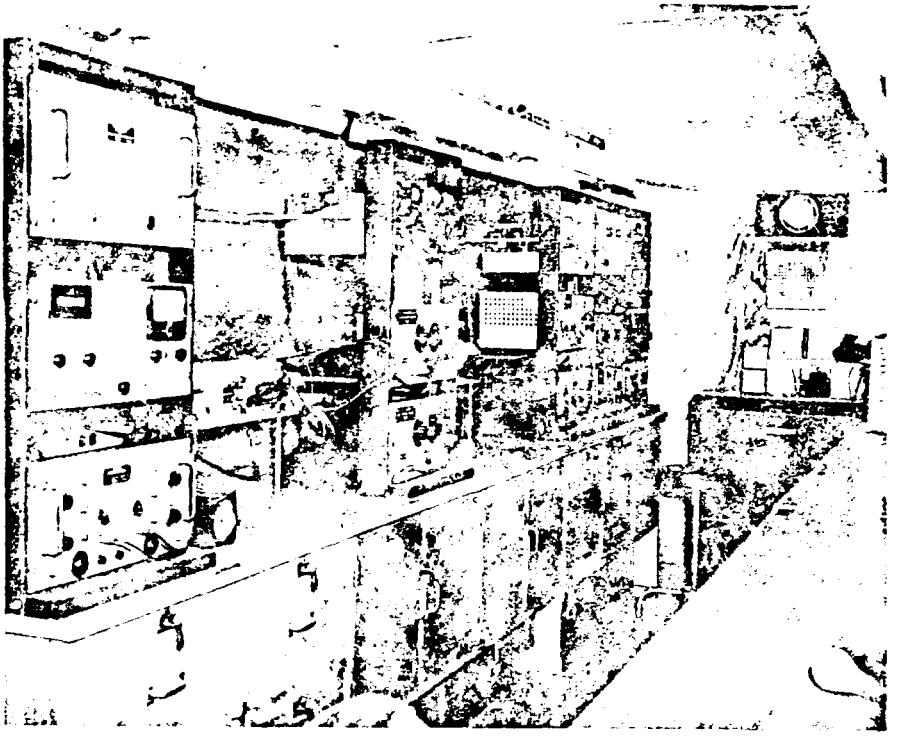

Fig. 2.9 Interior View of NRL Trailer

The equipment in this van included two complete scintillation spectrometers for [redacted] counting and a scintillation unit for counting the plutonium samples. A counting-rate meter was included to monitor the background as a protection against contamination of the unit. A supply of spare parts and tools was provided, so that the van served a secondary purpose as a stockroom.

The Signal Corps van was modified to the extent of replacing the original counting equipment with scalers and counters developed and tested at NRL. Its main equipment was the flow counters for handling the exposed gold samples.

Both of these trailers were located throughout the test series on Elmer.

The samples counted in the field were gold, [redacted] and plutonium. The remaining samples were flown to NRL for processing.

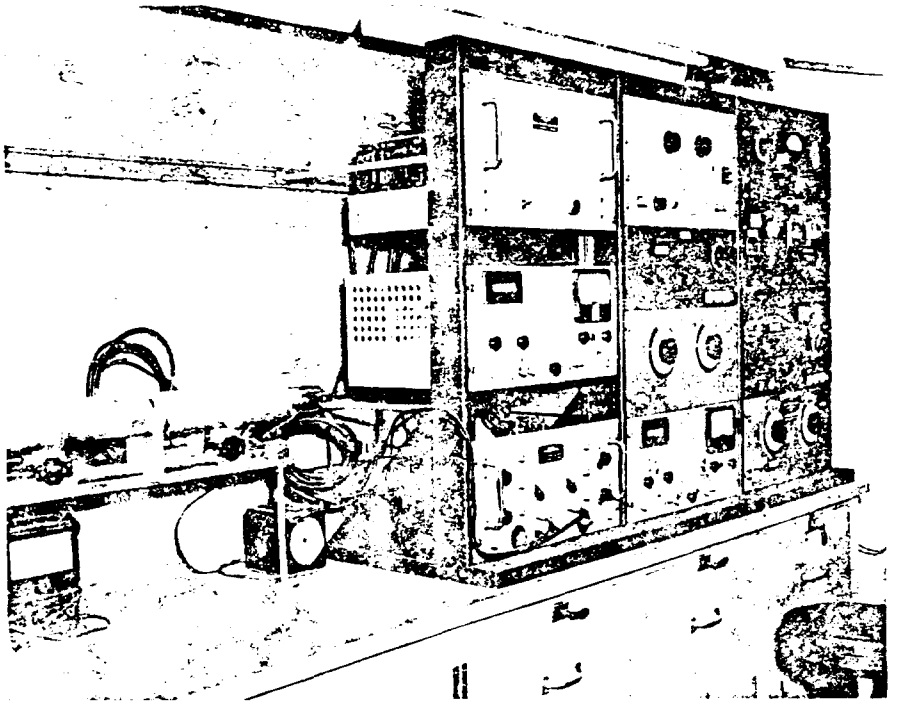

Fig. 2.10 Interior View of NRL Trailer

2.3 INSTRUMENTATION

The counting equipment used in this project will be treated in this section. Because of the diversity of the counting units, each will be discussed in a separate paragraph. It is felt that such a lengthy treatment is warranted on the basis that the technique will be of interest to the person reading this report and the fact that the accuracy of the reported measurements is entirely dependent on the reliability of the counting equipment described.

2.3.1 Sulfur Counters

The counting apparatus for those samples of relatively high counting rate, consists of an end window geiger tube, power supply and scaler. The geiger tube is mounted in a multiple sample holder so that 12 samples may be processed during one counting period. The scaler controls the count, recording, reset and sample changing automatically. An automatic print-register is included in the set-up to record the date, time, elapsed time of the count and the number of particles detected. Built into the print-register is a continuously running master clock and integral timer. In operation the scaler is usually set for preset count use, so that when the count is accumulated the stop pulse of

the scaler initiates the print cycle of the register which in turn provides a reset signal for the scaler and starts the drive motor on the sample rotator. When the sample table has turned one unit, a microswitch stops it and releases the relays holding the scaler and register in the reset state and the unit is ready for the second counting interval.

The convenience of this system is evident from the foregoing for it enables one to accumulate data continuously without the necessity of having an operator present at all times.

A more complete picture of this apparatus may be obtained by consulting Fig. 2.11.

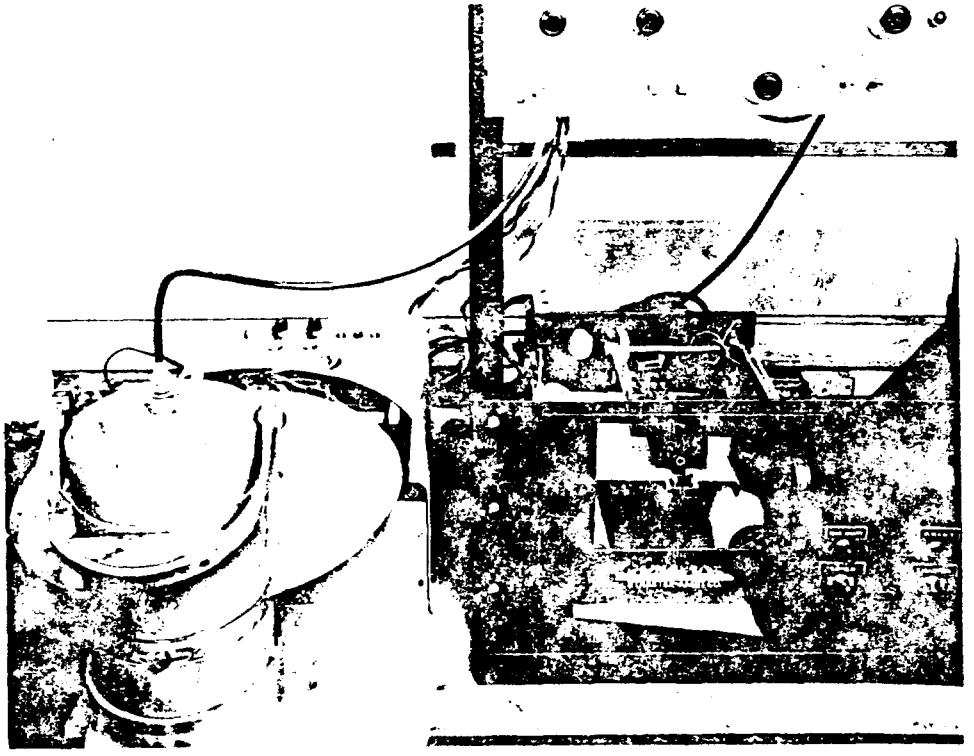

Fig. 2.11 Sulfur Counter

2.3.2 Anticoincidence Counters

These counters were originally designed to count sulfur samples of very low activity, in the region of a few counts per minute. With the ordinary geiger counter tube, surrounded by a nominal amount of lead or iron shielding, the background counting rate is still about 20 to 40 counts per minute. Because the neutron flux at ranges greater than 1000 yd from the normal weapon is relatively small above the threshold for sulfur, it became desirable to count activities lower than

the usual background. The method adopted to achieve this is to provide a shield of counter tubes around the principal counter. The shielding tubes are electrically coupled to the center tube in such a way that when both the shielding tubes and the center tube respond to an ionizing event at the same time, no count is recorded in the scaler. This is the so-called anticoincidence technique. The circuit is designed so that when the center tube alone responds to an event the resulting pulse is recorded by the scaler and is actually the result of activity of the sample being measured. It should be noted here that the samples counted on these systems are the tubular ones mentioned in the section describing the sulfur samples and their processing. Using this method it was possible to reduce the background to less than 4 C.P.M. The increase in overall sensitivity was calculated to be a factor of 111, by the following means:

$$\text{Sensitivity ratio} = \frac{\text{Cal. No. (end window tube)}}{\text{Cal. No. (anti. coin.)}} \times \frac{\text{Background (end window)}}{\text{Background (anti. coin.)}}$$

$$= \frac{7.18 \times 10^7}{4.15 \times 10^6} \times \frac{28}{7} = \frac{2010.4}{18.04} = 111$$

The counter tubes used in this apparatus are thin walled aluminum tubes. This type is necessary since the only radiation from the sulfur is beta radiation. The shielding tubes are arranged in a ring about 6 in. in diameter, there are a total of nine tubes in the ring. The counting tube is mounted in the center of the ring with its axis parallel to the axis of the ring. The entire assembly is in a lead jug the end of which opens to permit the samples to be inserted and removed with facility. Figures 2.12 and 2.13 give an overall view of this counting arrangement.

2.3.3 Continuous Gas Flow Proportional Counters

The counters used to process the gold samples are of the continuous gas flow type operated in the proportional region. These counters have an unlimited operating lifetime and excellent plateaus making them ideal for extended counting periods. Their one disadvantage is that they require the use of much higher voltages than the conventional geiger tube, operating in the region of 4000 volts as compared to under 1000 volts for the geiger tube. Because these counters are operated in the proportional region they require the use of a preamp and an amplifier; in the NRL systems a linear amplifier is built into the scaler making a very compact unit. The counter itself is one designed and built by Radiation Counter Laboratories MK-12 mod. 2,

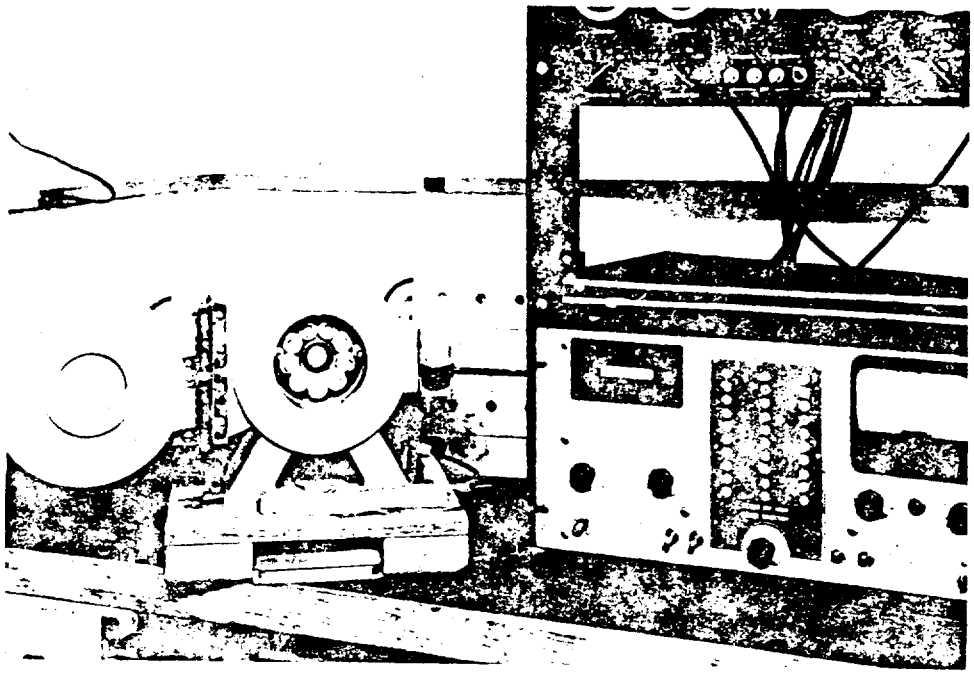

Fig. 2.12 Anticoincidence Counter

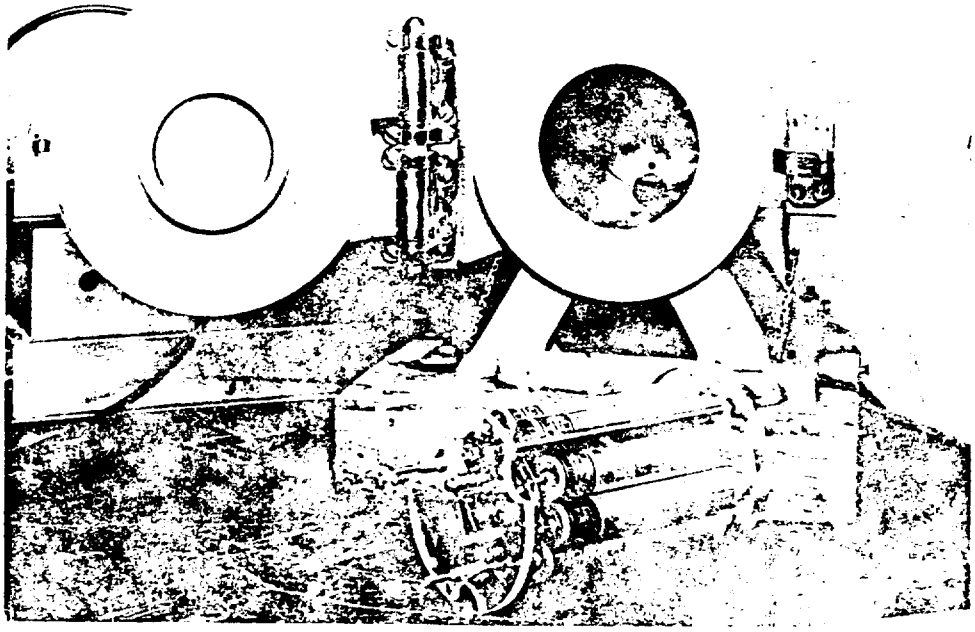

Fig. 2.13 Anticoincidence Counter

it contains three counting wells so that while one sample is counting another is in a chamber where it is flushed with gas, this is a time saving feature since a short wait is usually required after introducing a new sample to the counting volume to allow the gas to flush out any air in the counter. The third well is open to the operator for loading or unloading samples. The counting volume is approximately 1 inch in diameter and 1 1/2 inches long. The electrode is 1 mil wire bent in a loop 1/2 inch in diameter. These counters were chosen because they have a good plateau with pure methane gas rather than a helium, butane mixture and the pulse size is great enough in the proportional region to use a relatively low gain amplifier. It is quite possible that other units operating at lower voltage on a gas mixture would function as well, this group has not covered all the available types. (See Fig. 2.14.)

The operating plateau of this type counter is about 500 volts long and has a slope of approximately 3 percent per hundred volts. With the counter mounted in the lead shield as shown in Fig. 2.14 the background is reduced to 11 counts per minute. The scalers used with this counter have one microsecond input strips and one microsecond first scaling strips. There are no appreciable counting losses up to 1.6×10^4 counts per second.

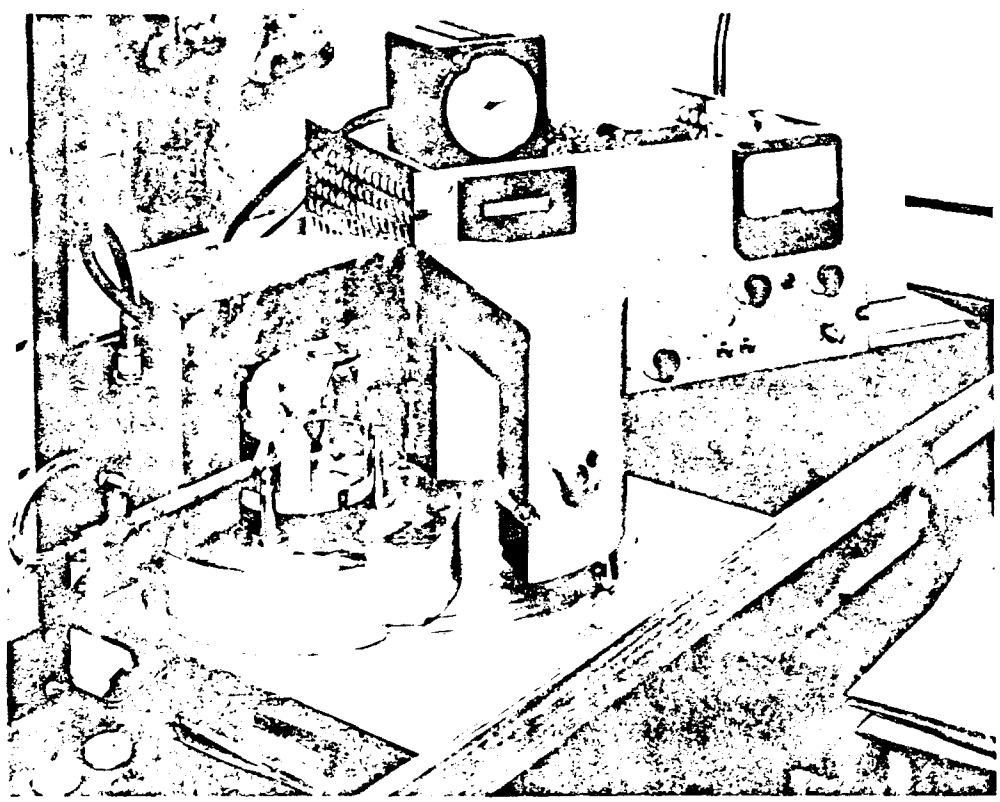

Fig. 2.14 Flow Counter

2.3.4 Scintillation Spectrometer

In order to facilitate the counting of the [ ], samples a gamma coincidence spectrometer was constructed. This unit consists of two 6292 photomultipliers and NaI(Tl) crystals mounted facing each other across a 1/4 in. gap, the output from each phototube is fed through its own preamp to a single channel analyzer (one for each tube). The outputs from the analyzers are fed to a coincidence circuit. The two channels are set so that they cover the region from 400 to 600 kev, bracketing the 511 kev line from the positron annihilation. At this setting the output from the coincidence circuit, as recorded on the scaler, is taken to be the count of the positron activity [ ] and is calibrated to give the neutron flux.

The two single channel analyzers and the coincidence circuit are constructed on one chassis making a very compact assembly. This design was originated by C. W. Johnston at LASL. The analyzers differ from the conventional types in that the pulse height selector and the "window" width are not independent; in this setup the pulse height is set and the "window" is set by raising the pulse height limit the desired number of volts above the pulse height threshold, i.e., if the threshold is set at 75 volts and the pulse limit is set at 80 volts then effectively the "window" width is 5 volts. Each analyzer has its own linear amplifier and a delay line is also provided so that it may be switched into one channel to check on the accidental rates. The singles rate from either channel may be checked by the same switch. The resolving time of the coincidence unit is 1 microsecond.

The sample to be counted is placed between the two crystals in a rigid mount to preserve the geometry of the system. A sodium-22 source is used as a standard source. Two of these units may be seen installed in the NRL trailer in Figs. 2.9 and 2.10.

2.4 EXPERIMENTAL PROCEDURE

2.4.1 Sample Calculation

Following is a sample of the type of calculation used to determine the neutron flux from the sample data.

The first step is the calculation of the initial counting rate of the sample. (I.C.R.)

$$\text{I.C.R.} = \text{C.R}_t \cdot e^{\lambda(t-t_o)}$$

where C.R._t is the counting rate at some time t, and λ is the disintegration constant for the particular half-life under consideration. The C.R._t is the average counts per minute of several counts taken, on both

top and bottom of the disc samples, this is done to average out direction effects and the chance misloading of these samples. The time t_o is the time of the weapon detonation.

Then:

$$\text{nvt} = (\text{I.C.R.}_{\text{unshielded}} - 1.025 \times \text{I.C.R.}_{\text{shielded}}) \times (\text{calibration no.})$$

This example shows the use of the cadmium difference technique used in the calculation of the thermal flux from gold or tantalum data. The factor 1.025 is the correction for epithermal neutrons absorbed in the cadmium shield. (That is 2 1/2% of the epithermals are absorbed in the 0.045 in. of cadmium surrounding the shielded samples.) For samples used to measure the higher energy neutrons the above equations reduce simply to the I.C.R. times a calibration number.

Several of the calibration numbers are listed below:

Gold - - - - - 8.16×10^5 neuts /cm^2 per count/min. (cd diff.)
Tantalum - - 2.31×10^8 neuts/cm^2 per count/min. (cd diff.)
Sulfur - - - - 7.18×10^7 neuts/cm^2 per count/min.

2.4.2 Calculation of Effect of Gamma Flux on Count Rate

Solving for a and b in these three equations one obtains:

$$a = \frac{c_1 c_3 - c_2^2}{c_1 \alpha^2 - 2c_2 \alpha + c_3}$$

$$b = \frac{2c_1 c_2 \alpha - c_1^2 \alpha^2 - c_2^2}{2c_2 \alpha - c_1 \alpha^2 - c_3}$$

The value "a" then becomes the corrected initial counting rate, and this number times the calibration number then gives the integrated neutron flux.

TABLE 2.2 - Shot 1 Data

Sample	Range (yd)	I.C.R. (Corrected)	Nvt	Nvt x R
Ta	2100	3.24×10^5	7.48×10^{13}	1.57×10^{17}
	2500	1.10×10^5	2.54×10^{13}	6.35×10^{16}
Au	2100	1.18×10^8	9.57×10^{13}	2.01×10^{17}
	2500	3.16×10^7	2.57×10^{13}	6.42×10^{16}

2.5 RESULTS

Table 2.2 lists the initial counting rates and calculated fluxes for the various samples exposed on Shot 1. The I.C.R.'s for gold and tantalum are actually the cadmium differences for those samples.

Figures 2.15 through 2.18 show the data from the various samples. These graphs are plots of the neutron flux (nvt) x R or R^2 versus the

range (R), depending upon the region of the energy spectrum covered by the detector. This type of plot is made to provide a straight line presentation which enables one to determine convenient parameters for describing the flux. The parameters generally used are the 1/e distance (so called e-fold) and the range = 0 intercept. These may be determined directly from the graphs.

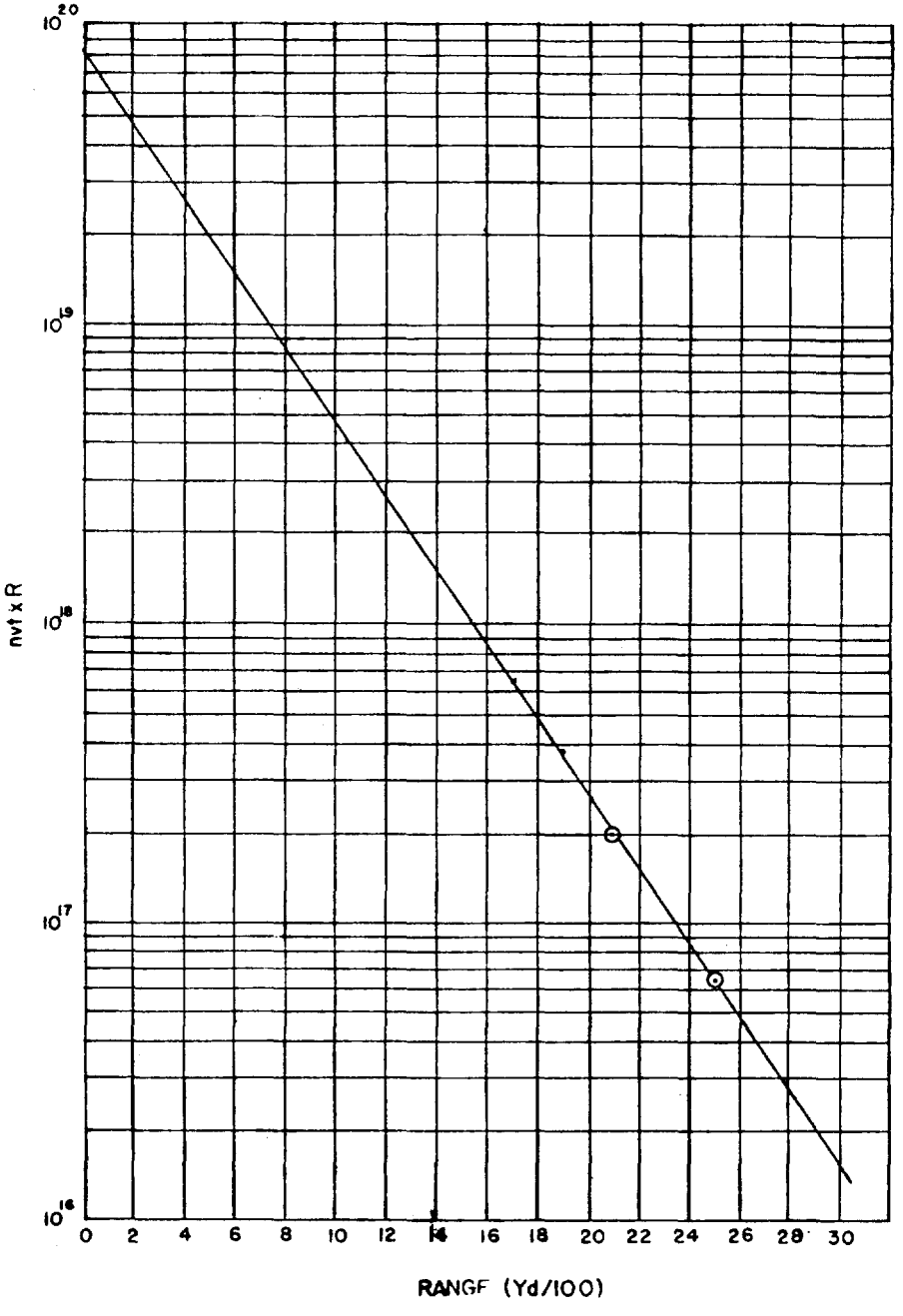

Fig. 2.15 Gold Data, Shot 1

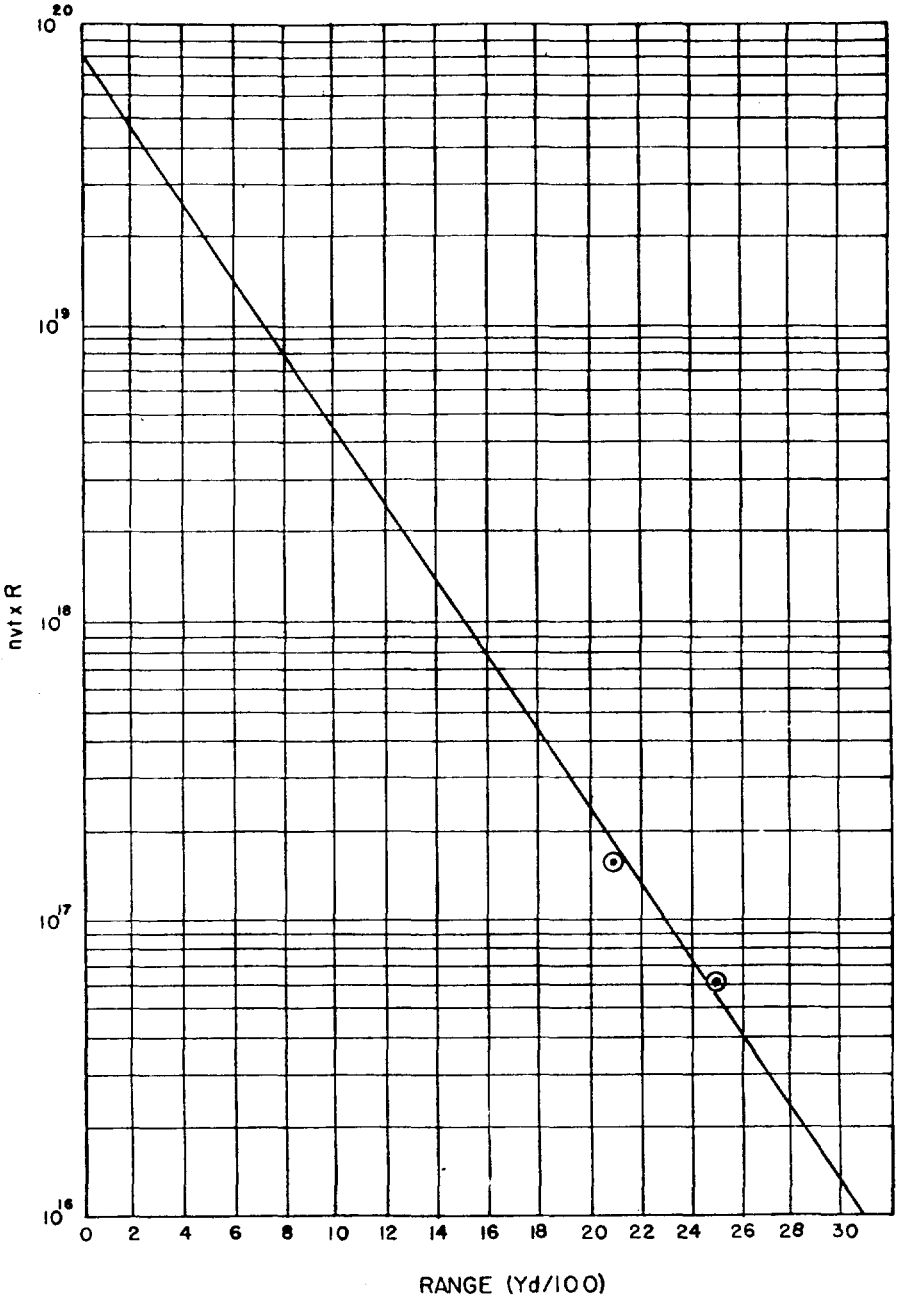

Fig. 2.16 Tantalum Data, Shot 1

Pages 35 & 36 Deleted.

The data acquired in this test series exhibit abnormally large e-fold distances in all but the case of [redacted] In previous tests, namely UPSHOT-KNOTHOLE and TUMBLER-SNAPPER, the data yielded e-fold distances of from 190-240 yd, where as the figures for the CASTLE data are in the region of 390 yd. A shorter e-fold distance was expected because of the fact that this series of tests were run at sea-level while those at the Nevada Proving Grounds were all at altitudes greater than 4000 ft. As may be seen from the graphs the curves are all based on two data points, except for the [redacted] this might account for the long e-fold distances (the scatter in two points being quite capable of producing this effect), if it were not for the other data acquired from different detectors. The uranium data given in Chapter 3 and the germanium data in Chapter 5, to a certain extent, also give evidence of the longer e-fold distances, thus tending to indicate that the fault does not lie in fact that there are only a small number of points on the flux curves. It is felt that the answer is contained in the experimental setup, either through some scattering phenomenon or in some diffusion or attenuation effect associated with the ball of fire generated by the device.

CHAPTER 3

MEASUREMENTS WITH FAST NEUTRON FISSION DETECTORS

3.1 PURPOSE AND GENERAL METHOD

The fission threshold detectors used in these tests consisted of electrodeposits of the oxides of U^{238}, Np^{237}, and Th^{232} faced against NTC nuclear plates. The nuclear plates were 25 microns thick and recorded the full residual range of any fission fragments that were produced in the deposits and entered into the emulsion. By microscopically counting fission track densities in the emulsion, applying absorption corrections, and using values for fast-fission cross-section listed in the literature, the number of neutrons above threshold energy that penetrated the area of the deposit could be deduced for each detector.

The primary purpose of this method was to obtain some knowledge of flux densities of neutrons in the energy-intervals (0.5 - 14 Mev) and (1.5 - 14 Mev) at various distances from several of the weapons used in the present tests.

3.2 DESCRIPTION OF DETECTORS

Pages 39 thru 41 Deleted.

Weighings were done with a Type FD1 analytical balance, Wm. Ainsworth & Sons, Inc. Denver, Colorado, using the method of swings. Individual weighings were found to be repeatable to within ± 7 micrograms with reasonable caution. Sample weights are given in Table 3.2, together with activities.

3.2.2 NTC Nuclear Plates

The nuclear plates used in these tests were from the same batch as those used by L. Fagg in UPSHOT-KNOTHOLE.[2] Sections were

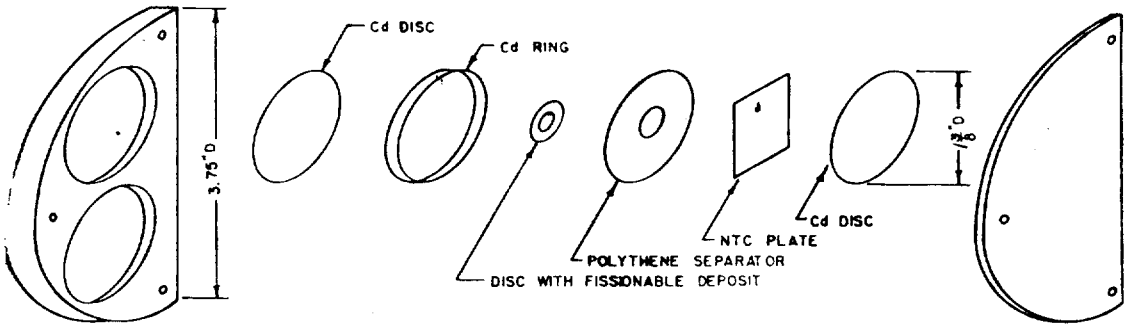

Fig. 3.1 Fission Detector Assembly

cut from 1 in. x 3 in. glass plates covered with Eastman-Kodak 25-microns thick NTC emulsion, and were fitted into cadmium or brass containers, as shown in Fig. 3.1.

The plates used were several years old and had been de-sensitized somewhat by remaining under refrigeration. Tracks of alpha particles were not recorded. L. Fagg made extensive tests to ascertain that alpha particles would not record on these emulsions at least within the range of developing techniques that might be used. A further check was made on these emulsions as part of the calibration experiment (next section).

A disc containing 100 μg per 0.44 cm^2 of natural uranium was placed against an NTC plate in the calibration experiment and remained in contact for 17 days. Since the activity of the discs was 80 counts/min, 340 alpha particles had impinged on the nuclear plate per 107-micron diameter field of view. None of these alpha particle tracks were observed during scanning for fission fragments; the fission fragment track density on this same plate was about 1 track per field of view.

All plates exposed to the alpha emitting discs were found to have a high density of developed grains within the first 2 microns of surface. This density seemed to be proportional to the amount of alpha-radiation exposure. Due to delays in recovery, this surface density was so great that it had to be removed from some of the field exposed plates before sufficient illumination and discrimination could be had (see Sec. 3.4.2.).

Samples of NTC plates were exposed to gamma intensities up to 2000 r from a cobalt-60 source. No evidence of appreciable increase in background grain density due to these exposures was discernible. From this, it was concluded that gamma intensities inside the detector stations would not affect experimental results.

The plates were developed by the following procedure:

Development - 10 minutes in Kodak D-19
Wash - 2 minutes in distilled water
Fix - 30 minutes in 30 per cent $Na_2S_2O_3$

The above times were found not to be critical. The plates used in the field experiments were coated with a protective film of motion picture lacquer after drying. During development, some of the emulsions were loosened from the glass backing and had to be spread carefully on the glass again during drying. The area of the image was sometimes stretched and had to be remeasured for use in data analysis.

Plates were scanned with a Leitz ortholux microscope, using 12x periplan eyepieces and a 100x apochromatic oil-immersion objective. A 6 x 6 square graticule was fitted into the left eyepiece to allow ease of counting high track densities. Calibration with a stage micrometer showed that the diameter of the field of view was 106.8 microns and the area of a field of view was 8.96×10^{-5} cm^2.

3.2.3 Detector Assembly and Calibration

The detector assembly consisted of the 10 mil thick, 1.3 cm diameter platinum disc, containing a 17 mm diameter (0.442 cm^2) fissionable deposit; a 4 mil thick polyethylene separator, 3.4 cm in diameter with a 9.5 mm D hole through the center; an NTC coated nuclear plate, about 2 cm x 2 cm; a 1/32 in. thick cadmium (or brass) container for the fission disc and nuclear plate, consisting of a ring 3.5 cm in diameter and 0.3 cm wide with front and back discs to fit inside the ring and enclose firmly the fission disc against the plate; an outer brass container to contain two cadmium containers and give further protection against heat or shock. The inner cadmium containers were held together with black photographic tape; the outer containers were held together with three screws and were made light tight with photographic tape. The fission discs were held in position by Scotch-taping them to the polyethylene separators which fitted tightly into the cadmium containers. A few neptunium detectors were exposed in inner brass containers to ascertain whether thermal neutron flux levels were really unimportant to the experimental design. A disassembled view of a detector is shown in Fig. 3.1.

This calibration will be used in the data analysis, Sec. 3.5.2, to determine the effective thickness, b, of undeveloped surface deposit in which no track grains can be discerned, and it will be important in calculating fractional self-absorption of fission fragments in the deposits.

3.3 LOCATION OF FIELD INSTALLATIONS

The detectors were placed in the bunker stations[18] on island Able, or in the wide flange stations (see Fig. 2.7) as listed in the Table 2.1. A view of the geometry of the detector in the bunker station is shown in Fig. 3.2.

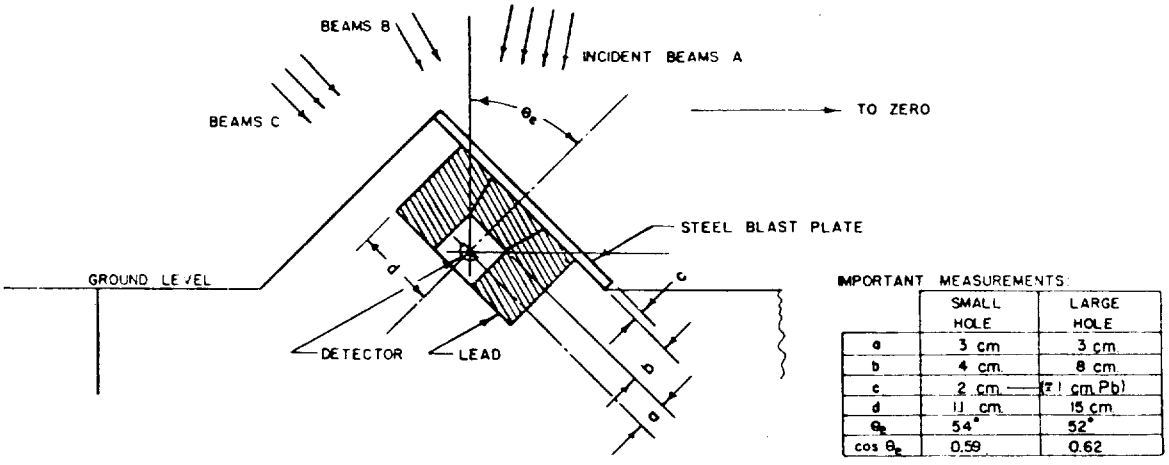

IMPORTANT MEASUREMENTS:

	SMALL HOLE	LARGE HOLE
a	3 cm	3 cm
b	4 cm	8 cm
c	2 cm	(7.1 cm Pb)
d	11 cm	15 cm
θ_z	54°	52°
cos θ_z	0.59	0.62

Fig. 3.2 Schematic of Detector in Bunker Station

3.4 RECOVERY AND PROCESSING OF DATA

3.4.1 Recovery

Recoveries were made after residual radiation had reached a level that precluded exposure of any individual to more than 3.8 r during the entire operation. Therefore, samples from Shot 1 were not recovered and processed until 2 weeks after the shot, giving a total exposure of

the plates to alpha radiation of 42 days. Plates from Shot 2 were exposed to alphas for 50 days. The recovered samples and their locations are given in Table 3.3.

TABLE 3.3 - Presentation of Data

Station and Detector	Range (Yd)	No. Fission Tracks Counted >4 grains	Number of Detectable Tracks	Fraction of Fissions Detectable	Total Fissions in Deposit
Shot 1					
14.03.03,U12	2000	1117 ± 34	5.37×10^3	0.098 ± 0.018	$5.47 \pm 0.99 \times 10^4$
14.03.03,N18	2000	71 ± 8.4	1.48×10^5	0.318 ± 0.041	$4.65 \pm 0.84 \times 10^5$
Shot 2					
14.03.06,U7	1650	126 ± 11.2	8.72×10^3	0.075 ± 0.014	$1.16 \pm 0.25 \times 10^5$
14.03,06,N2	1650	115 ± 10.7	9.22×10^5	0.310 ± 0.041	$2.97 \pm 0.48 \times 10^6$
14.03.06,N17	1650	106 ± 10.3	6.30×10^5	0.171 ± 0.040	$3.68 \pm 0.92 \times 10^6$
14.03.03,U14	1950	76 ± 8.7	870	0.107 ± 0.019	$8.14 \pm 1.71 \times 10^3$
14.03.03,T4	1950	4	110	0.102 ± 0.019	$\sim 10^3$
14.03.03,N26	1950	117 ± 11	3.80×10^5	0.195 ± 0.039	$1.95 \pm 0.43 \times 10^3$
14.03.02,N29	2050	287 ± 17	1.10×10^5	0.166 ± 0.039	$6.62 \pm 1.65 \times 10^5$
14.01 ,U16	2450	96 ± 9.8	2.72×10^5	0.150 ± 0.027	$1.81 \pm 0.38 \times 10^4$

3.4.2 Processing

After recovery, the detectors were disassembled and the plates were developed according to the procedure of Sec. 3.2.2. It was found that in some cases, particularly the highly active neptunium detectors, the surface grain density was so great that not enough light could penetrate the plate to allow the focusing of the emulsion underneath. In all cases the darkness of the emulsion surface that had been opposite the deposit was about proportional to the alpha dose received. Also, this surface density was limited to a 2-micron layer after development. Areas of the emulsion surrounding the deposit were transparent indicating that gamma radiation did not cause the darkening. Emulsions that were exposed to highly active alpha emitters or extreme gamma intensities did require extra caution to discriminate against random grain alignment.

In all deposits, the surface layer of grains due to alpha bombardment was removed before track-counting by lightly-rubbing with a chamois soaked in xylene. Care was taken to remove no more of the surface than required to allow discrimination of fission tracks. After the plates were rubbed, they were allowed to dry for a few minutes before scanning.

3.4 3 Methods of Scanning

All data were obtained on the Leitz Ortholux microscope with 12x Periplan eyepieces and a x100 Apo Oel objective. Shillaber's immersion oil, Grade A, was used as a medium between emulsion and lens. The field of view with the above lenses was measured with a stage micrometer to be 106.8 microns in diameter and 8.96×10^{-5} cm^2.

Plates with many tracks per field of view were scanned by selecting enough fields scattered around the area of the image to give good statistics and a representative coverage of the image. Tracks were counted only if they were 5 grains or more in length and if they seemed to originate at the surface of the emulsion. Of course, the part of the track which lay within the heavy surface layer of grains could not be discriminated, and therefore this surface layer had to be considered in calculating effective absorption of the fragments (see Sec. 3.5.2). When 5 random grains aligned and were not definitely recognized as a track, closer scrutiny was required. In these cases, the characteristic close-spacing of grains at the end of a fission track, and the larger size of track grains compared to colloidal silver grains, had to be taken into account in deciding whether the track was produced by a fission fragment. In plates with higher density of background grains, this discrimination was more difficult and led to larger uncertainties in track count.

3.4.4 Presentation of Data

The data obtained in terms of total tracks counted, and the calculated value of total tracks produced are presented in Table 3.3.

3.5 TRANSLATION OF DATA TO RESULTS

3.5.1 General Considerations

As mentioned in Sec. 3.2.1, deposits were selected of thicknesses that allowed considerable fractional absorption of fission fragments produced. Moreover, the presence of a 2-micron surface layer of the emulsion in which tracks were not identifiable further reduced the fraction of fission fragments produced that was seen in the emulsion. Therefore, in data analysis it was first necessary to translate the fraction of fission fragments counted to total number of fissions produced in the fissionable deposit. Next, the proper fission cross-sections were selected to convert fissions produced to total neutron flux within the detector station. Then, the proper scattering cross section had to be determined for converting neutrons read by each threshold detector into incident fluxes outside the station. And finally,

the fractional solid angle of incidence was estimated from multiple neutron scattering phenomena to estimate total neutron fluxes and doses at a point outside of each detector station.

3.5.2 Fractional Absorption of Fission Fragments by Deposit

An analysis[15] of the problem of fission fragment absorption in a deposit leads to the following equations for the fractional number of fissions that produce recognizable tracks:

Case I

$$F = \frac{Q}{NT} = \left[1 - \frac{1}{2}\left(b + \frac{aT}{2}\right)\left(\frac{1}{C_l} + \frac{1}{C_h}\right)\right], \quad T \leq r_{eh}, \tag{3.4}$$

Case II

$$F = \frac{1}{T}\left\{r_{eh}\left[1 - \frac{1}{2}\left(b + \frac{ar_{eh}}{2}\right)\left(\frac{1}{C_l} + \frac{1}{C_h}\right)\right] + \frac{1}{2}\left[\left(1 - \frac{b}{C_l}\right)\left(T - r_{eh}\right) - \frac{a}{C_l}\left(\frac{T^2}{2} - \frac{r_{eh}^2}{2}\right)\right]\right\},$$

$$r_{eh} < T \leq r_{el} \tag{3.5}$$

Case III

F = (same as above, with T replaced by r_{el} in the second [ ]),

$T > r_{el}$ (3.6)

where the symbols represent:

- a - ratio of linear stopping powers, deposit to emulsion,
- b - thickness of insensitive layer of emulsion,
- C - $ar_o - R_r'$, where r_o is the linear range of a fragment in the deposit and R_r' is the minimum detectable range in undeveloped emulsion.
- C_l, C_h - values of C for the light and heavy fragments, respectively,
- F - fractional number of fissions in deposit that produce recognizable tracks in the emulsion,
- N - number of fissions produced per unit thickness of deposit,
- Q - number of tracks produced in the emulsion by fissions within the layer, O-T,

r_{el} - "effective" range of light fragment in deposit, equal to $r_{ol} - \frac{R'_r}{a} - \frac{b}{a}$,

r_{eh} - "effective" range of heavy fragment in deposit, equal to $r_{oh} - \frac{R'_r}{a} - \frac{b}{a}$,

r_{ol}, r_{oh} - total ranges in deposit of light and heavy fragments, respectively,

T - Thickness of deposit.

Assuming a density of 7.3 gm/cm^3 for U_3O_8 and extraneous deposit, the following values of parameters were obtained:

$a = 9.7$; $C_l = ar_{ol} - R'_r = 9.7\,(1.48) - 4 = 11.3$ microns;

$C_h = ar_{oh} - R_{r_l} = 9.7(1.15) - 4 = 7.1$ microns; $\left(\frac{1}{C_l} + \frac{1}{C_h}\right) = 0.2295$ microns^{-1};

$F = 0.213$ for detector UC calibration (see Sec. 3.2.3); a value of

$T = \frac{2.03 \times 100}{0.442 \times 7.3 \times 10^6}$ cm $= 0.62$ microns for detector UC; and a value

$b = 3.46$ microns from successive approximations using $F = 0.213$;

$T = 0.62$ microns, Equations 3.4 and 3.5, and the definitions of r_{el} and r_{eh}.

Considerations in the selection of some of the above parameters were as follows:

Each fission was assumed to produce symmetrically[19,20] fragments of mass 143 and 96, and of energy 65 Mev and 97 Mev, respectively. The ranges in emulsion of these heavy and light fragments from uranium are taken from Demers.[21] The emulsion ranges for heavy and light fragments are, respectively:

$R_h = 11.14$ microns,

$R_l = 14.32$ microns.

The value of R_h agrees with that calculated from the equation[22,23]

$$R = R_a \frac{7A_l}{(Z_{eff})^2} \qquad (3.7)$$

where

R_a - range of alpha particle of the same initial velocity,

A_l - mass of fragment, 143

Z_{eff} - effective charge on fragment, 22 in electronic units[24]

For an energy of 65 Mev, the fragment has an initial velocity $v = \sqrt{\frac{2E}{M}} = 9.3 \times 10^8$ cm/sec. An alpha particle with this velocity has a kinetic

energy of 1.81 Mev, and a range[25] of 6 microns in emulsion. Substituting these values in Equation 1.4 gives R = 12.6 microns, which is close to that obtained by Demers.

According to Segrè and Weigand[27] 2.7 mg/cm^2 of U_3O_8 is equivalent in absorbing power to 1 mg/cm^2 of Al, and 1 micron of emulsion is equivalent to 0.028 mg/cm^2 of Al.[21] From these values the range table, Table 3.4, is constructed.

TABLE 3.4 - Ranges of Fission Fragments

Range	Light Fragments	Heavy Fragments
Emulsion (microns)	14.32	11.14
Emulsion (mg/cm^2)	0.558	0.434
Aluminum (mg/cm^2)	0.401	0.312
U_3O_8 (mg/cm^2)	1.083	0.842
U_3O_8 (microns, ρ = 7.31)	1.48	1.15

The ratio of the total linear stopping powers of fission fragments in deposit and emulsion was taken as the inverse ratio of ranges listed in Table 3.4:

$$a = \frac{Sd}{Se} = \frac{\text{stopping power of } U_3O_8}{\text{stopping power of emulsion}} = \frac{11.14}{1.15} = 9.7$$

The range in undeveloped emulsion, R_r', corresponding to a minimum grain length of 5 grains was measured under the microscope to be 4 ± 1 microns.

The value of b was determined from Equations 3.4 and 3.5 by successive approximations of b and r_{eh} using the 14-Mev calibration of detector UC in terms of detectable tracks/neutron (Sec. 3.2.3); the measured value,[28] 1.2 barns, for the fast neutron fission cross section for U^{238} for 14-Mev neutrons; the radiometrically determined weight of uranium on disc UC of 100 μg; and the average ratio of total deposit weight to uranium weight from the 12 weighed uranium discs, 2.03 ± 0.31.

From the calibration, the fraction, F, of fissions causing detectable tracks in detector UC may be calculated:

The absorption coefficient is

$$\mu = 1.2 \times 10^{-24} \text{ cm}^2/\text{atom} \times \frac{6.02 \times 10^{23}}{238} = \text{atoms/gm}$$

$$= 3.05 \times 10^{-3} \text{ cm}^2/\text{gm}.$$

The fraction of neutrons above the uranium threshold that are incident and produce fissions is:

$$\mu T = 3.05 \times 10^{-3} \times \frac{100\ \mu g \times 10^6}{0.442\ cm^2} = 6.9 \times 10^{-7}$$

Thus,

$$F = \frac{\text{detectable tracks/cm}^2}{\text{neutron flux} \times 6.9 \times 10^{-7}}$$

$$= (\text{from Sec. 1.2.3}) \frac{1.12 \times 10^4}{7.62 \times 10^{10} \times 6.9 \times 10^{-7}}$$

$$= 0.213$$

Using this value of F, a UC deposit thickness of $2.03 \times \frac{100}{0.442} = 460\ \mu g/cm^2 = 0.62$ microns (U_3O_8 density is 7.3), the fission fragment ranges listed in Table 3.4, and a required residual range, R_r', of 4 microns in undeveloped emulsion, the value b = 3.46 microns was calculated by Equations 3.4 and 3.5 as described above. In developed emulsion this thickness would shrink to $\frac{10}{25} \times 3.5 = 1.4$ microns, which agrees reasonably with the rough focusing-vernier measurement of the thickness of the dense surface layer of grains. This value of b was used together with Equations 3.4, 3.5, and 3.6 in calculating the fractional number of fission fragments counted from each of the experimental detectors. This calculation should be the most accurate for the uranium detector since each of these detectors was weighed separately and the above parameters apply to U_3O_8 films. However, the densities and stopping powers of the neptunium and thorium deposits should be close to those of uranium. Therefore, the ranges and parameters for uranium deposits were assumed applicable to the neptunium and thorium deposits. The calculated values of fractional fission fragment detection are listed in Table 3.3.

3.5.3 Effective Detector Thresholds

Effective detector thresholds and cross sections were estimated averages from the data of reference 28. The values selected are given in Table 3.5. In absence of pretest knowledge of the shapes of the neutron spectra, the neutrons detected by fast-fission were assumed to be mostly in the region above the initial threshold and before the second, or roughly between 1 and 6 Mev. The effective threshold energies represent the energy at which the fast-fission cross section reaches 1/2 the plateau value. For fission spectrum neutrons, a mean fast neutron fission cross section of 0.306 barns has been calculated.[29]

TABLE 3.5 - Fast Fission Detector Thresholds

Element	Threshold Region (Mev)	Plateau (Mev)	Effective Threshold (Mev)	Average σ_f (barns)
Uranium-238	1.4 - 2.0	2.0 – 6.0	1.45	0.55
		7.0 – 14.0	Unimportant	1.1
Neptunium-237	0.5 - 1.5	1.5 – 6.0	0.64	1.5
		7	-	2.6
Thorium-232	1.4 - 2.2	2 – 6	1.5	0.15
		data not available above 6 Mev		

3.5.4 Calculation of Flux Inside Bunker Station

The neutron fluxes as measured inside the detector stations were calculated by the relation

$$N = \frac{DA}{\sigma_f \, W \, 6.02 \times 10^{23}} \text{ neutrons/cm}^2 \qquad (3.8)$$

where symbols are:

σ_f - fast neutron fission cross section, cm^2,
D - total number of fissions in deposit,
W - weight of fissionable element in deposit, grams,
A - gm-atomic weight of fissionable element, grams.

As an example, consider detector U12. The nuclear plate was scanned by strips 104 microns wide at intervals of 500 microns. The number of tracks counted was 1117 ± 34, giving a total number of observable tracks of $(500/104) \times 1117 = 5370 \pm 138$, due to fissions in the adjacent deposit. Since deposit U12 contained 183 μg of U^{238} and a total deposit of 365.7 ± 7.0 μg, an absorption correction, as calculated by the method given in Sec. 3.5.2, of $[0.0982]^{-1}$ gives a total number of fissions 5.47×10^4, Taking the effective cross section from Table 3.5 to be 0.55×10^{-24} cm^2, the neutron flux inside the 4-cm lead-shielded hole of station 14.03.03 was, according to Equation 3.8,

$$N = \frac{5.47 \times 10^4 \times 238}{0.55 \times 10^{-24} \times 184 \times 10^{-6} \times 6.02 \times 10^{23}}$$
$$= 2.13 \times 10^{11} \text{ neutrons/cm}^2.$$

3.5.5 Attenuation Introduced by Station

In Fig. 3.2 is given a schematic view of the location of a detector within a bunker station. The detector is essentially shielded on all sides by adequate thicknesses of concrete, and is shielded in front by, in most cases, the 4-cm thick lead plug and the 1/2 in. steel plate. It is assumed for the problem of calculating station attenuation, and it is justified in Appendix A, that the neutron flux incident on the detector station is practically isotropic both in numbers and energy. This results because the stations are many mean free paths for collision of neutrons in air. Assuming an average total cross section for N_2 and O_2 of 1.75 barns, the mean free path is about 120 yd.

Since the mean free path is long compared to the dimensions of the station, there will be no intense multiple scattering in the air close to the station. Therefore, considering the flux to be isotropic, neutrons arrive at the detector station in the following ways (see Fig. 3.2);

A. From beams within some effective half angle θ_e.

B. From beams incident to the lead plug at angles where $\theta_e < \theta < 90^o$ to the axis of the detector well. These beams are necessarily narrower than those of A, and moreover, will scatter a relatively small fraction of neutrons in the lead plug toward the detector at such large scattering angles.

C. From beams incident at angles greater than 90^o to the axis of the well. These beams will be considered totally absorbed by the surrounding concrete.

Only the beams A will contribute significantly to the fast neutron flux inside the station. The processes by which neutrons from beams A enter the station and arrive at the detector are as follows:

(1) Neutrons penetrate to the detector without interaction.

(2) They are scattered coherently in the lead mostly within angle[30] $\theta_o = \frac{\lambda}{R}$ where λ is the neutron wave length divided by 2π, and R is the radius of the lead nucleus, 8.7×10^{-13} cm. For 3 Mev neutrons, $\theta_o = 109^o$. Since the detectors were so close to the lead plugs, it is assumed that elastic scattering away from the detector is compensated for by elastic scattering toward the detector from parts of the beam not originally traveling toward the detector. (Also see reference 33 for the results of beams incident to detectors enclosed in lead spheres.)

(3) Neutrons incident within half-angle θ_e are scattered incoherently in the lead plug. A large fraction of these are reduced to energies below the threshold of the detector and are scattered almost isotropically in the laboratory system. However, from the data of Phillips et. al., a considerable fraction of 14 Mev neutrons scattered inelastically in lead spheres was detected by a threshold detector responding to neutrons greater than 2 Mev. This suggests the

TABLE 3.6 - Inelastic Scattering Cross Sections in Lead

Detector Threshold (Mev)	Incident Neutron Energy (Mev)	Total Inelastic Cross Section (barns)	$\sigma_{in}(E_n,E_t)$ Inelastic Cross Section $<E_t$ (barns)	Reference
0.5	1.5	2.81	0	32
0.75	3.0	2.76	0.7	32
0.9	1.5	2.81	0.4	32
1.0(U^{238})	2.5	-	0.55	32
1 (U^{238})	Rn-Be	-	1.34	41
1.50	3	2.76	1.2	
2	14	2.77	0.91 ± 0.06	42 & 32
	3.7	2.57 ± 1.0		43

consideration of an "effective" inelastic cross section $\sigma_{in}(E_n,E_t)$, which includes only scatterings that produce neutrons below threshold level. It is assumed, as in elastic scattering, that the geometry of the detector station makes scattering toward and away from the detector mutually compensatory. The $\sigma_{in}(E_n, E_t)$'s used in absorption calculations were selected from data listed in Table 3.6, for 2-3 Mev incident neutrons, and the selected σ's are presented below:

Element	Threshold (Mev)	$\sigma_{in}(E_n, E_t)$ (barns)
Uranium-238	1.45	0.9 ± 0.2
Neptunium-237	0.64	0.7 ± 0.2
Thorium-232	1.5	0.9 ± 0.2

Using the selected values of $\sigma_{in}(E_n, E_t)$ the mean absorption of neutrons incident to the lead plug within half-angle θ_e was calculated as shown in Appendix B. The multiplying factors to convert measured detector fluxes to fluxes incident to the station within a cone of half-angle θ_e are presented for each detector in Table 3.7.

3.5.6 Fluxes Outside Station

To estimate the total neutron flux above ground near each detector station, it was again assumed that the flux was isotropic after 15-20 mean free paths. Although the coral ground occupied nearly half the solid angle subtended at the detector station, it will be assumed that scattering of neutrons from the ground makes the effective fraction of neutrons incident from directions outside the cone of half-angle θ_e the

TABLE 3.7 - Conversion Factors for Station Attenuation

	Detector	Mean Atten. Corr.	Solid Angle* Geom. Corr.	Total Multiplying Factor
LARGE WELL	U & Th	1.40 ± 0.56	5.3 ± 1.3	7.4 ± 3.5
8 cm pb plug	Np	1.30 ± 0.53	5.3 ± 1.3	6.9 ± 3.3
SMALL WELL	U & Th	1.21 ± 0.23	4.9 ± 1.2	5.9 ± 1.8
4 cm pb plug	Np	1.15 ± 0.22	4.9 ± 1.2	5.6 ± 1.7

*Error represents maximum fixed error estimated as one-half of the lower 2π solid angle.

same as it would be if the station were located in an infinite medium of air. Obviously this assumption would be more valid if the weapon were detonated at greater height and if the ratios and angular distributions of scattering and absorption were the same in the coral as in air. Factors to convert fluxes within an effective cone of half-angle θ_e to total fluxes also are presented in Table 3.7, together with the overall conversion factors for converting fluxes inside stations to fluxes outside. The doses given to a point receiver near each station were estimated, assuming[34] 1.4×10^7 neutrons/cm^2 per Rem in the 3-Mev region and 2.8×10^7 n/cm^2 per Rem in the 1 Mev region, and are presented in Table 3.8 together with total fluxes.

TABLE 3.8 - Summary of Results

Station and Detector*	Distance (D) (yd)	Flux (F_i) Above Threshold Inside Station (n/cm^2)	F_iD^2 (n-cm^{-2}-yd^2)	Flux F_o Above Threshold Outside Station (n/cm^2)	F_oD^2 (n-cm^{-2}-yd^2)	Dose Above Threshold (rem)
SHOT 1						
14.03.03,U12	2000	$2.13 \pm 0.38 \times 10^{11}$	$8.52 \pm 1.53 \times 10^{17}$	$1.26 \pm 0.45 \times 10^{12}$	$5.04 \pm 1.81 \times 10^{18}$	$9.0 \pm 3.3 \times 10^4$
14.03.03,N18	2000	$1.26 \pm 0.23 \times 10^{12}$	$5.04 \pm 0.91 \times 10^{18}$	$7.06 \pm 2.54 \times 10^{12}$	$2.82 \pm 1.01 \times 10^{19}$	$2.5 \pm 0.9 \times 10^5$
SHOT 2						
14.03.06,U7	1650	$4.38 \pm 0.92 \times 10^{11}$	$1.19 \pm 0.25 \times 10^{18}$	$2.58 \pm 0.96 \times 10^{12}$	$7.02 \pm 2.60 \times 10^{18}$	$1.84 \pm 0.68 \times 10^5$
14.03.06,N2	1650	$7.90 \pm 1.30 \times 10^{12}$	$2.15 \pm 0.34 \times 10^{19}$	$4.43 \pm 1.50 \times 10^{13}$	$1.20 \pm 0.41 \times 10^{20}$	$1.58 \pm 0.54 \times 10^6$
14.03.06,N17	1650	$6.74 \pm 1.70 \times 10^{12}$	$1.83 \pm 0.46 \times 10^{19}$	$3.78 \pm 1.47 \times 10^{13}$	$1.03 \pm 0.40 \times 10^{20}$	$1.35 \pm 0.53 \times 10^6$
14.03.03,U14	1950	$3.00 \pm 0.63 \times 10^{10}$	$1.14 \pm 0.24 \times 10^{17}$	$1.77 \pm 0.65 \times 10^{11}$	$6.72 \pm 2.48 \times 10^{17}$	$1.3 \pm 0.5 \times 10^4$
14.03.03,T4	1950	1.5×10^{10}	5.7×10^{16}	8.86×10^{10}	3.4×10^{17}	6.3×10^3
14.03.03,N26	1950	$3.81 \pm 0.84 \times 10^{12}$	$1.45 \pm 0.32 \times 10^{19}$	$2.13 \pm 0.81 \times 10^{13}$	$8.10 \pm 3.08 \times 10^{19}$	$7.6 \pm 2.9 \times 10^5$
14.03.02,N29	2050	$1.20 \pm 0.30 \times 10^{12}$	$5.04 \pm 1.26 \times 10^{18}$	$6.72 \pm 2.62 \times 10^{12}$	$2.83 \pm 1.10 \times 10^{19}$	$2.4 \pm 0.9 \times 10^5$
14.01,U16	2450	$7.58 \pm 1.59 \times 10^{10}$	$4.55 \pm 0.96 \times 10^{17}$	$4.47 \pm 1.65 \times 10^{11}$	$2.68 \pm 0.99 \times 10^{18}$	$3.2 \pm 1.2 \times 10^4$

*Pre-fixes U, N, and T of detector numbers indicate U^{238}, Np^{237}, and Th^{232} detectors, respectively. The results of detectors N18 and N17 contain additional uncertainties as a result of the great non-uniformity of the deposits in these detectors.

3.6 SUMMARY OF RESULTS

3.6.1 Presentation

The results of the fission threshold measurements are summarized in Table 3.8. The number of detectable tracks listed represents the total number that could have been counted under the criterion of counting tracks greater than 4 grains in length. The number of fissions was derived from the total number of tracks by the methods of Sec. 3.5.2. See Sec. 3.4.4 for data presentation. The fluxes represent the total number of neutrons of energy greater than threshold energy that passed through an area of 1 cm^2, inside and outside the stations. The dose from neutrons above threshold for each detector is estimated in terms of roentgen-equivalent-mammal[35] (rem), where the flux of 2-3 Mev neutrons equivalent to 1 rem is taken as 1.4×10^7 neutrons/cm^2 and the flux of 1-Mev neutrons/cm^2 equivalent to 1 rem is taken as 2.8×10^7 n/cm^2.[34] Fluxes inside the stations are plotted as a function, $F_i D^2$ versus D in Fig. 3.3. Fluxes outside the stations are plotted similarly in Fig. 3.4, and dose versus distance is plotted in Fig. 3.5.

The Shot 2 uranium curve of Fig. 3.3 was assumed to be a straight line, and was drawn through the most reliable point (U7), minimizing the sum of the squares of the deviations of the other two points (U14 and U16). Likewise, the Shot 2 neptunium line was drawn through N2, minimizing the sum of the squared deviations of N26 and N29. Since the U12 Shot 1 point is much more reliable than the N18 point (see Table 3.8), the estimated Shot 1 uranium curve was drawn through U12 and parallel to the Shot 2 uranium curve. However, the N18 point was ignored in drawing the estimated Shot 1 neptunium curve; instead, this curve was drawn parallel to the Shot 2 neptunium curve in such manner that the neptunium flux ratios would be the same as the uranium flux ratios for the two shots.

The corresponding $F_o D^2$ curves of Fig. 3.4 were drawn parallel to those of Fig. 3.3. The Shot 2 curves were again drawn through the points of U7 and N2, respectively, and approximately the same flux ratios between the two shots were preserved. The dose curves of Fig. 3.5 were fitted to the experimental points using extra points calculated from the straight lines of Fig. 3.4.

3.6.2 Discussion

The overall errors listed for neutron fluxes include statistical and estimated fixed errors of the experimental method used in these measurements, and also the uncertainities in the parameters selected from the literature. An attempt was made to include all errors that would lead to the over-all probable error obtaining if these

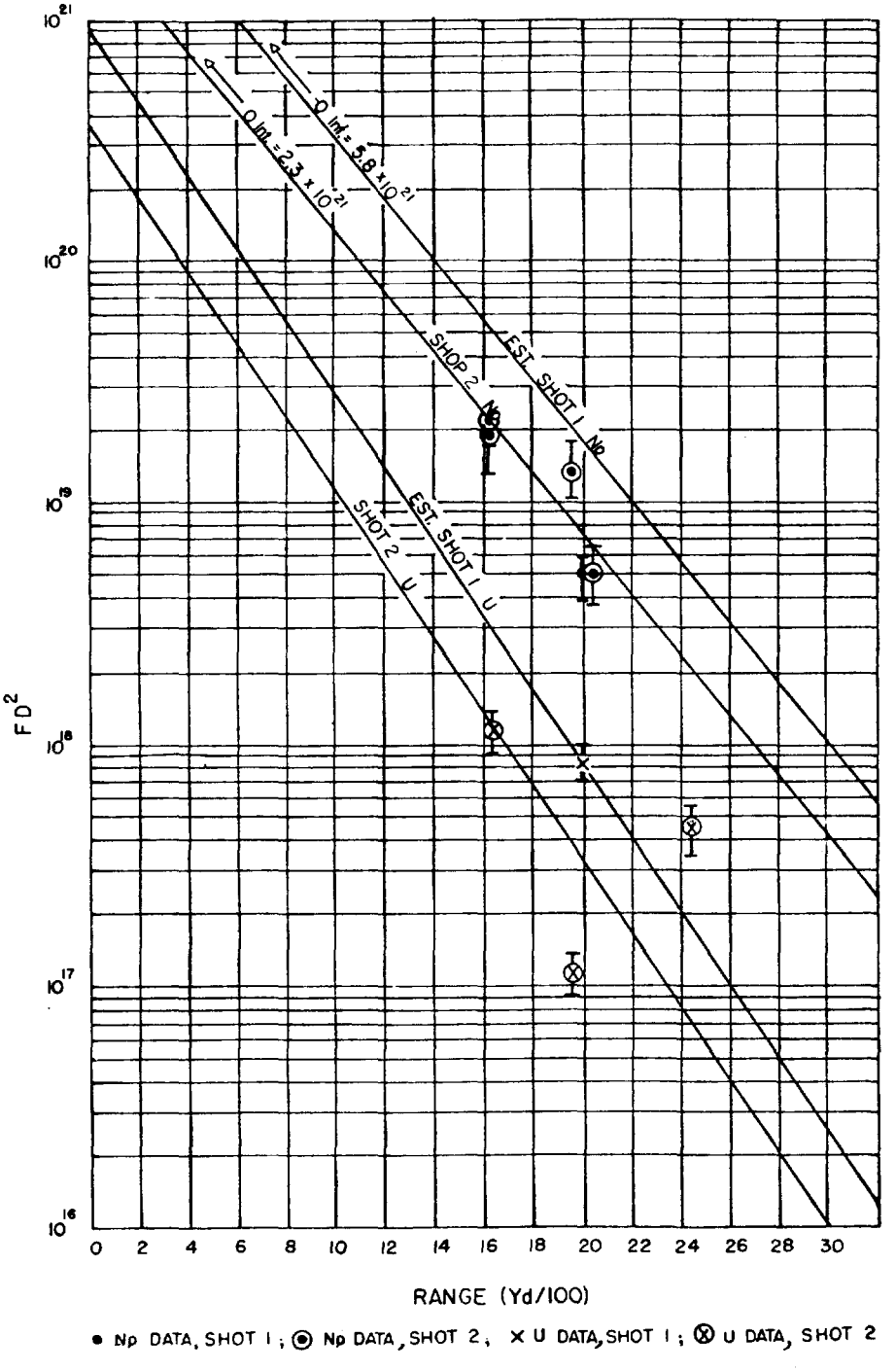

Fig. 3.3 Flux Inside Stations

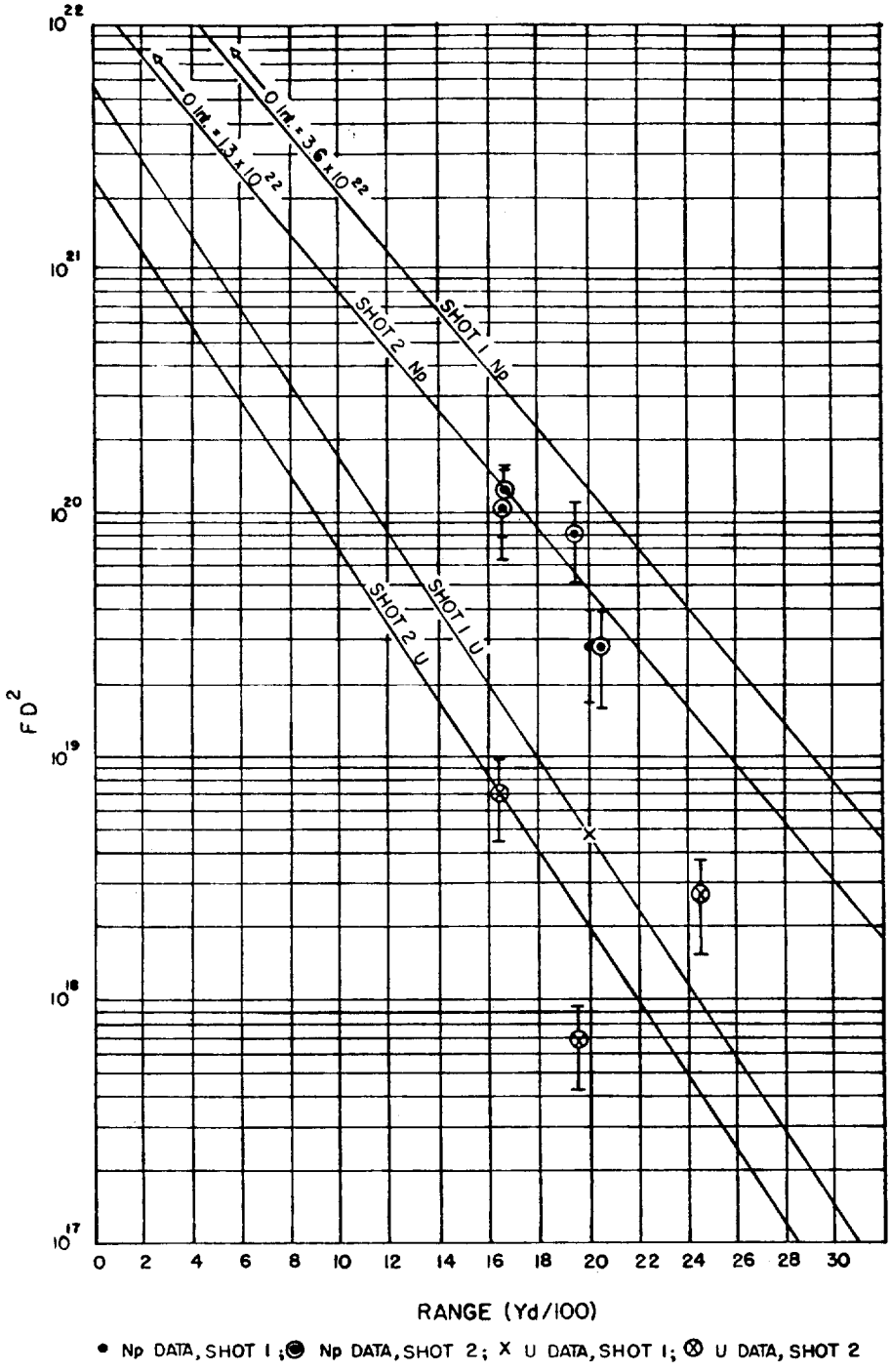

Fig. 3.4 Flux Outside Stations

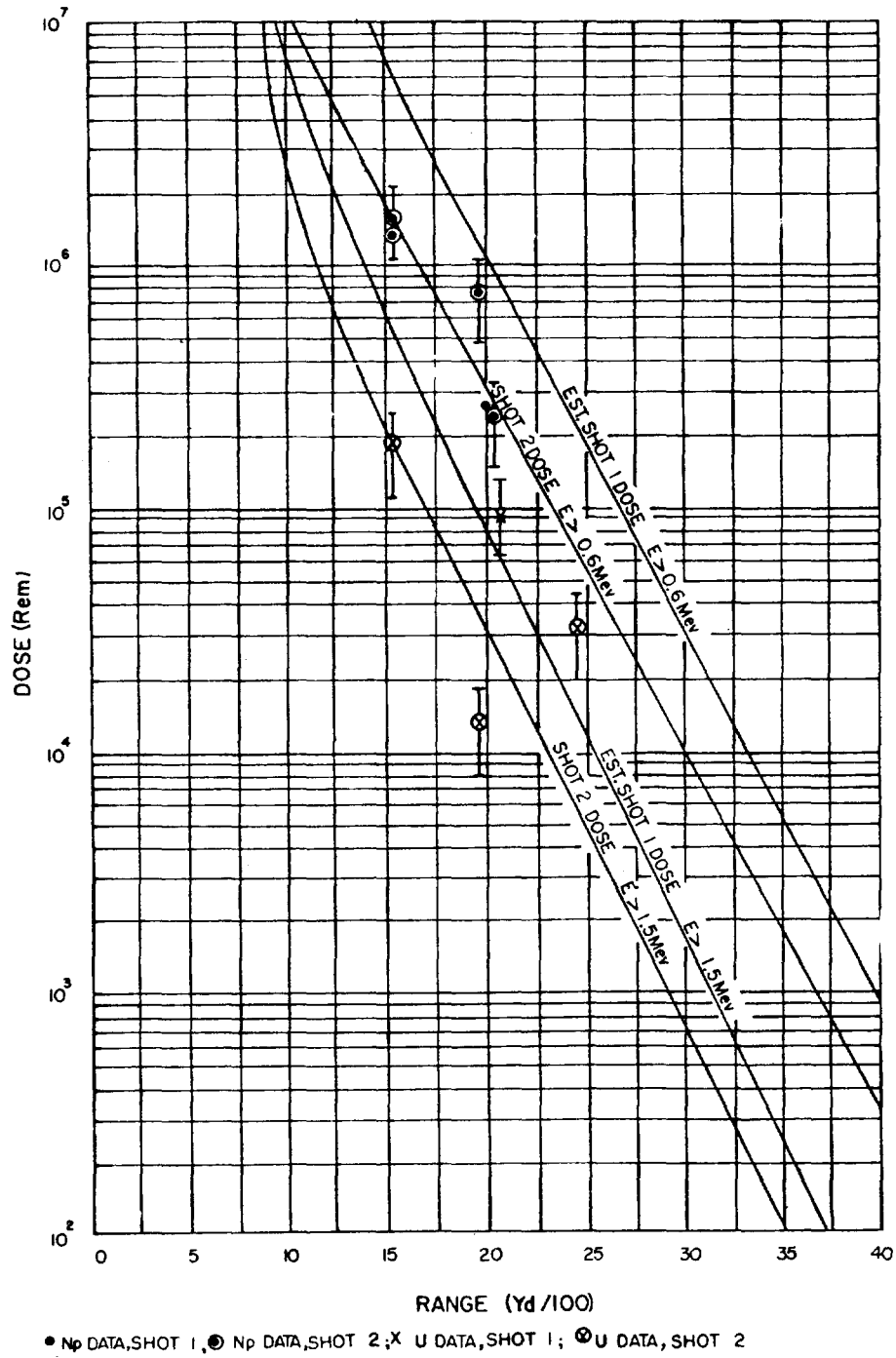

Fig. 3.5 Neutron Dose Vs. Distance

measurements were made by a number of individuals using the same procedures given herein. However, additional errors due to uncertainties of position of samples in the stations, and to scattering and absorption by other samples, were difficult to estimate and are not included. These effects may explain the considerable departure of some of the points from the straight line FD^2 curves.

The greater part of the error listed in the table of results is composed of fixed errors due to not accurately estimable fission-fragment absorption, or to radiation attenuation by the detector stations. These fixed errors would not change appreciably with distance and would be expected to lie in the same direction (plus or minus). Therefore, the slopes of the curves of flux versus distance are probably more accurate than would be indicated if the errors of the points were purely statistical.

Since there are large uncertainties in the measured fluxes and in the "effective" thresholds of the fission detectors, it is difficult to estimate the differential flux or dose due to neutrons in the energy interval between the neptunium and uranium thresholds, However, the results indicate that the majority of the neutrons with energies greater than 0.5 Mev have energies lying in the region 0.5-2.0 Mev.

The brass-enclosed N17 detector gave the same reading as the cadmium-enclosed N2 detector, showing that thermal fluxes had no effect on experimental results. The T4 thorium detector was the only thorium detector recoverable and its track density was sparse; however, the track density checked roughly the results of the U14 detector.

The doses listed at each station estimate the fast-neutron doses, in terms of roentgen-equivalents of biological damage, that would be received by a point receiver near the station. Small animals would receive nearly this dose at all parts of their bodies. A man in such isotropic fields would receive fractional amounts of less than half of these doses at various organs within his body, due to the shielding provided by one part of the body for another. Figure 3.5 shows that from Shot 1 a neutron dose of 100 rem was received at 4200-4400 yd; from Shot 2, 100 rem was received at 4100-4300 yd.

Assuming an exponential attenuation in air, the curves of Figs. 3.3 and 3.4 lead to an e-fold distance of 290 yd for neutrons of the spectrum recorded by the uranium detectors. The neptunium detector measurements lead to an e-fold distance of 350 yd. The y-axis intercepts in Fig. 3.3 for Shot 2 uranium, Shot 1 uranium, Shot 2 neptunium, and Shot 1 neptunium are 3.7×10^{20}, 8.8×10^{20}, 2.3×10^{21}, and 5.8×10^{21}, respectively. The correspondingly y-intercepts in Fig. 3.4 are 2.3×10^{21}, 5.4×10^{21}, 1.3×10^{22}, and 3.6×10^{22}, respectively.

It may be noted that the fluxes at 2000 yd from Shot 1 were about 1000 times the estimated minimum in Table 3.1. Those from Shot 2 were 400 times the estimated minimums. Moreover, the fluxes did not

decrease as rapidly with distance as predictions had indicated. Extrapolating the neptunium curves of Fig. 3.4 to 1 yd and assuming isotropic sources, the total fast neutron yields of the Shot 1 and Shot 2 devices were about 4.5×10^{23} and 1.6×10^{23}, respectively.

A recommended improvement in the procedure used herein, in view of the appreciable amounts of extraneous deposit encountered and the difficulty of observing fission fragment tracks in the first few microns of emulsion surface, is that deposit thicknesses be held to a maximum of 100 micrograms/cm^2 of the fissionable element. Other important considerations in future applications of the fissionable deposit nuclear plate technique are: (1) The plates should be exposed to the alpha-emitting deposits no longer than necessary; (2) Tests should be made to ascertain that the nuclear plates do not record alpha-particles or that they at least provide easy discrimination between fission-fragment tracks and alpha tracks---plates may be de-sensitized if necessary,[26] (3) A calibration should be made with monoergic neutrons of energy where the fission cross-sections are well known for the detectors used. The methods of Sec. 3.5.2 are generally applicable for the determination of deposit self-absorption and the thickness of any insensitive surface layer of emulsion, or other absorber, that may have to be accounted for. An important advantage of the methods of this section are that they are unaffected by the intensities and energies of the gamma radiation encountered in weapons tests. With the above precautions, the methods outlined in this section could be used in the future with better accuracy than was attainable in the present tests. Furthermore, due to the small size of the sensitive part of the detecting instrument, and its ability to withstand gamma intensities of the 10,000 r level, it would be possible at the greater ranges to take measurements subtending any desired solid angle of space without introducing any neutron shielding other than that required for blast and heat protection.

PART II

NEUTRON MEASUREMENTS BY DETECTION OF FISSION PRODUCT GAMMA RAYS

CHAPTER 4

EXPERIMENT DESIGN

4.1 PRINCIPLES OF OPERATION

The measurement of neutron intensity, spectrum, and tissue dose with fission threshold detectors was developed and used at UPSHOT-KNOTHOLE, Spring, 1953.[44] This report covers further development of this method and its use at CASTLE, Spring, 1954.

The purpose of these measurements is to give information on the neutron intensity and spectrum from an atomic device in the region between thermal energy and 2.5 Mev. This energy region includes a large majority of the neutrons formed in the primary fission process and the number of neutrons in this region can exceed the remaining number by one or more orders of magnitude, depending on the type of device and the distance of the point of measurement from the device. Although the tissue dose per neutron increases with neutron energy, the large number of neutrons in this intermediate region causes them to contribute the major part of the neutron tissue dose.

The method consists of exposing suitably encased samples of fissionable material to the incident radiation. Neutrons cause fissions to take place in the samples. The samples are recovered and the gamma rays resulting from the decay of the fission products are detected and counted. The counting rate at a given time can be related to the number of fissions which occurred in the sample, and knowledge of the sample weight and fission cross section enables the neutron intensity to be calculated. The use of materials with different fission

threshold energies and a relatively constant cross section above the threshold makes possible a rough measurement of the spectrum of the incident neutrons. The tissue dose (rep) which would be received can then be calculated from the spectrum.

4.2 SAMPLES, CROSS SECTIONS, AND THRESHOLDS

The fissionable materials used were Pu^{239}, Np^{237}, and U^{238}. The table below gives the fission cross sections and thresholds. The values used are discussed in the previous paper.[44]

Sample*	Idealized Threshold	Average Cross Section (barns)	Average Sample Weight (gms)
Pu^{239}	200 ev(a) 1000 ev(b)	2.0	1.0
Np^{237}	.75 Mev	1.5	.050
U^{238}	1.50 Mev	0.43	.66

(a) Surrounded by 5.5 gm/cm^2 of normal B_4C.
(b) Surrounded by 2.9 gm/cm^2 of pure B^{10}.

*We are indebted to Dr. Jane Hall of LASL Laboratory for the preparation of the Pu samples, and to B. Harmatz and G. W. Parker of Oak Ridge National Laboratory for the U and Np samples, respectively. All samples were sealed in lucite holders, 1 in. in diameter and 1/8 in. thick.

4.3 SAMPLE HOLDERS

The sample holder used for Pu and U is shown in Fig. 4.1 and the one for Pu and Np in Fig. 4.2. They were constructed with 1/4 in. mild steel walls and filled with pulverized B_4C, packed to a density of 1.74 gm/cc or powdered metallic B^{10} packed to 1.50 gm/cc. These holders were fastened to 5/8 in. steel plates which in turn were fastened to the concrete bunkers for steel "H" frames discussed in Sec. 2.2.1.

4.4 COUNTING SYSTEMS

In order to detect the fission product gamma rays with maximum sensitivity, the inherent gamma rays from the sample (approximately 0.4 Mev from Pu, 0.3 from Np) must be discriminated against. To

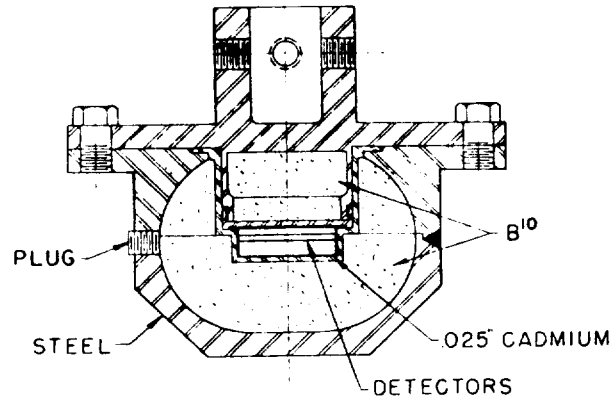

Fig. 4.1 Sample Holder for Pu and U

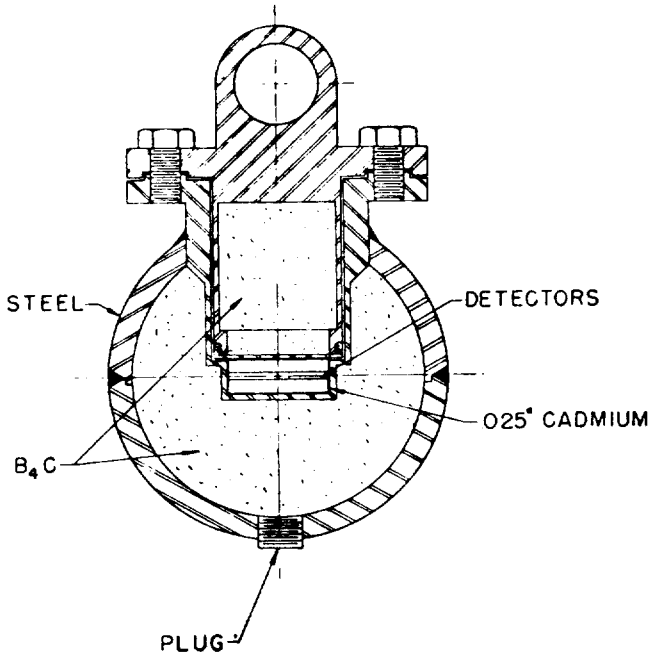

Fig. 4.2 Sample Holder for Pu and Np

accomplish this a scintillation counter with a NaI(Tl) crystal and an integral pulse height discriminator are used. A lead filter between sample and crystal gives further discrimination against the (relatively) low energy gamma rays from the samples by taking advantage of the increase in the absorption coefficient with decrease in gamma ray energy.

It should be noted that no chemical or physical treatments of the samples are required before counting and that samples may be reused after a suitable decay period.

The field equipment used at CASTLE, shown mounted in the trailer-van in Figs. 2.9 and 2.10, consisted of two independent systems, each containing the following: Harshaw X6L4 1-1/2 in. x 1 in NaI(Tl) crystal and Dumont 6292 photomultiplier with preamplifier in a 4 in. thick lead shield, Fluke 400 C power supply (operated at 900 volts), Atomic 204B linear amplifier, Atomic 510 single channel analyzer (operated as an integral discriminator) and an Atomic 1050 decade scaler and register. This system has operated quite satisfactorily and seems to have the desired characteristics of energy resolution, sensitivity, stability and reliability for field usage.

4.5 OPERATING CONDITIONS

To determine the optimum conditions for counting each of the samples for discriminating against the inherent gamma ray activity, the data shown in Fig. 4.3 were taken. The curves show the counting rate versus integral pulse height discriminator settings (PHS) for the total background of the unirradiated samples and for fission product gamma rays 15 hr after exposure of Pu to thermal neutrons (Pu sample background subtracted). These data were all taken with a 1/4 in. Pb cap over the crystal.

It can be seen that the sensitivity of the system (defined as the ratio of the count rate due to fission products to the count rate due to sample background) is a maximum for Pu at PHS 45. The sensitivity is nearly constant for Np above PHS 30 and for U above PHS 15. In order to get high counting rates and still allow for drifts in the counting system, the settings chosen were 35 for Np, 20 for U, and 45 for Pu.

A similar set of curves taken with a 1/2 in. Pb filter showed a slightly lower sensitivity and the counting rates were lower by about a factor of two.

The pulse height discriminator was calibrated in terms of gamma ray energy by taking differential pulse height curves with Cs^{137} and Co^{60} sources. The resolution and peak/valley ratio for Cs^{137} were 9 per cent and 20, respectively.

In terms of the gamma ray energy, Pu was counted by observing the fission product gamma rays with an energy above 0.81 Mev, Np those above 0.62 Mev and U those above 0.34 Mev.

In addition to maximum sensitivity (or "signal/noise ratio"), the optimum operating conditions chosen have other advantages. The relatively high background counting rate means that good counting statistics may be obtained with reasonably short counting times. Also,

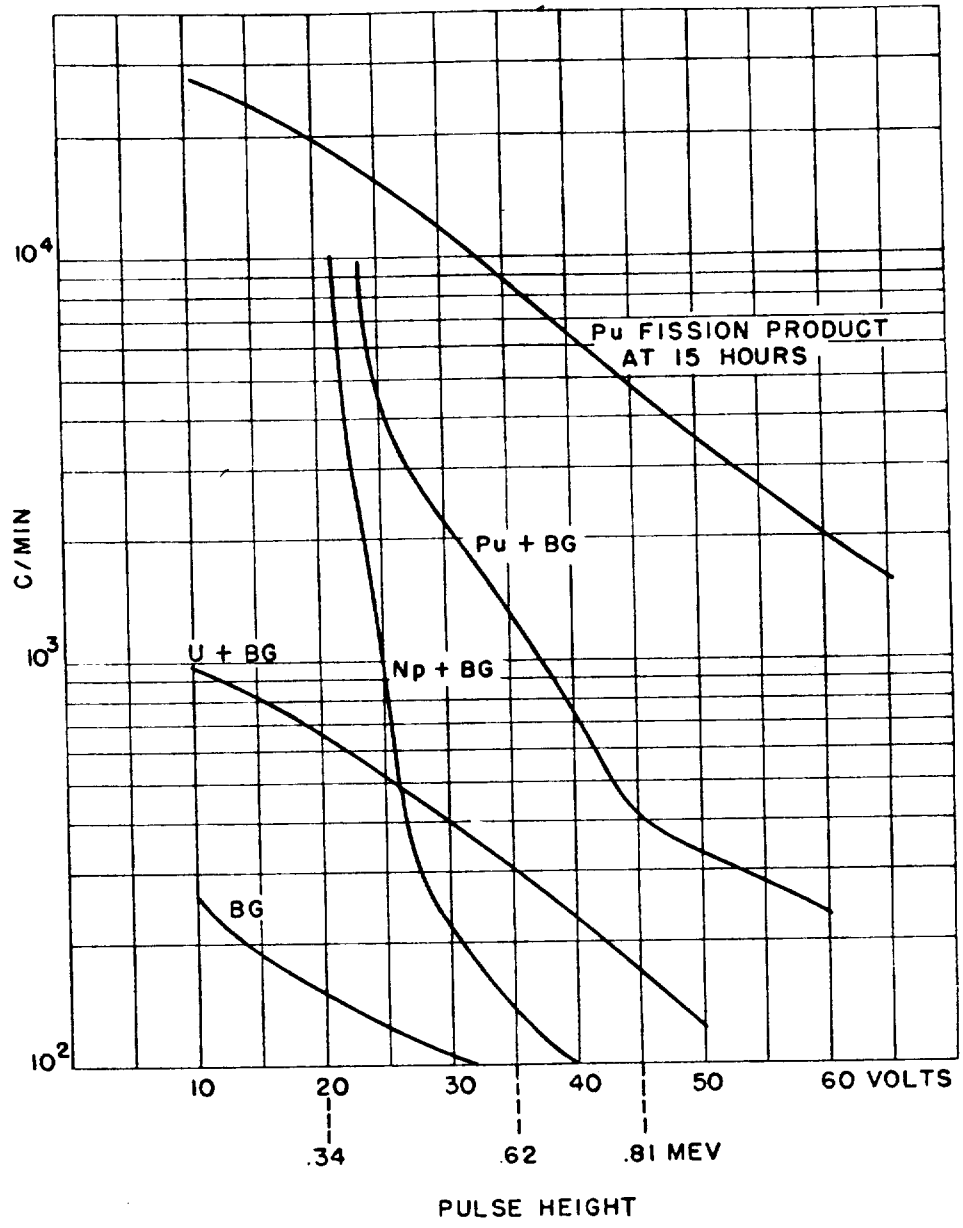

Fig. 4.3 Integral Spectra

since the background from the sample itself is several times greater than the natural background (counter plus atmospheric), fluctuations in the latter are of relatively minor significance.

4.6 CALIBRATION

Calibration of the counting system is accomplished by taking advantage of the relatively high Pu fission cross section for thermal

neutrons. (Thermal neutrons are eliminated in the field measurements by boron shielding.) A Pu sample is exposed to a known thermal neutron flux and the counting rate of the sample is determined, as a function of time after irradiation, at the PHS determined in Sec. 4.4. Since the fission cross sections, sample weights, and thermal neutron flux are all either well known or easily measured, the calibration of the system is relatively simple and accurate.

Calibration was carried out in the thermal neutron flux of the ORNL graphite reactor. The flux was measured using gold foils, as discussed in Sec. 2.1.1, with both the ORNL and NRL standard counting systems.

Due to the high thermal neutron cross section of Pu (700 barns) it is necessary to use a smaller sample (0.1 gm) for calibration in order to have a "thin" absorber and avoid large flux perturbations. The sample calculation below illustrates the calibration procedure.

0.105 gm Pu exposed for 600 sec at 5.61×10^7 thermal n/cm^2 sec. Ten hours later, the net counting rates were 35,500 c/min at PHS 20, 16,000 at PHS 35, and 7700 at PHS 45. Thus, the counting rate at PHS 35 for 10^{10} fast neutrons/cm^2 on 1 gm of Np would be

$$\frac{16{,}000 \text{ c/min}}{5.61 \times 10^7 \text{ n/cm}^2\text{sec} \times 600 \text{ sec}} \times \frac{1.5 \text{ barns (Np, fast)}}{700 \text{ barns (Pu, therm)}} \times \frac{1 \text{ gm Np}}{0.105 \text{ gm Pu}} \times 10^{10}$$

or 97.1 (c/min)/(10^{10} n/cm^2) for 1 gm of Np at 10 hr after exposure. The calibration curve obtained in this manner is given in Fig. 4.4.

The decay of the gamma ray activity by a power law relationship of the form $C\,Kt^{-x}$ is primarily due to the statistical nature of the fission process, as discussed by Way and Wigner.[45] A difference from the usually quoted $t^{-1.2}$ is not unexpected since this relation is valid (approximately) for N(E)EdE, the total energy liberated by the fission products, while this experiment measured $E_B N(E)\,(E)dE$, where E_B is the bias energy and (E) is the efficiency of the NaI(Tl) crystal as a function of gamma ray energy.[46] A power law relation with x = 1.30 has been observed at low bias (0.3 Mev) from 1 hr to, at least, 250 hr after exposure. As the bias energy is raised, x increases and is 1.72 at 1.0 Mev for the first 30 hr after exposure. The faster decay rate at higher energy is due to the general fact[45] that the higher energy transitions have shorter half lives.

At the bias of 0.81 Mev used for counting Pu, x = 1.63 from 0.5 to 45 hr, at which time there is a very sharp break in the curve (Fig. 4.4) with x 0.72 from 50 to 250 hr. A change in the power law exponent with time is reasonable at a high bias in that fewer fission products are

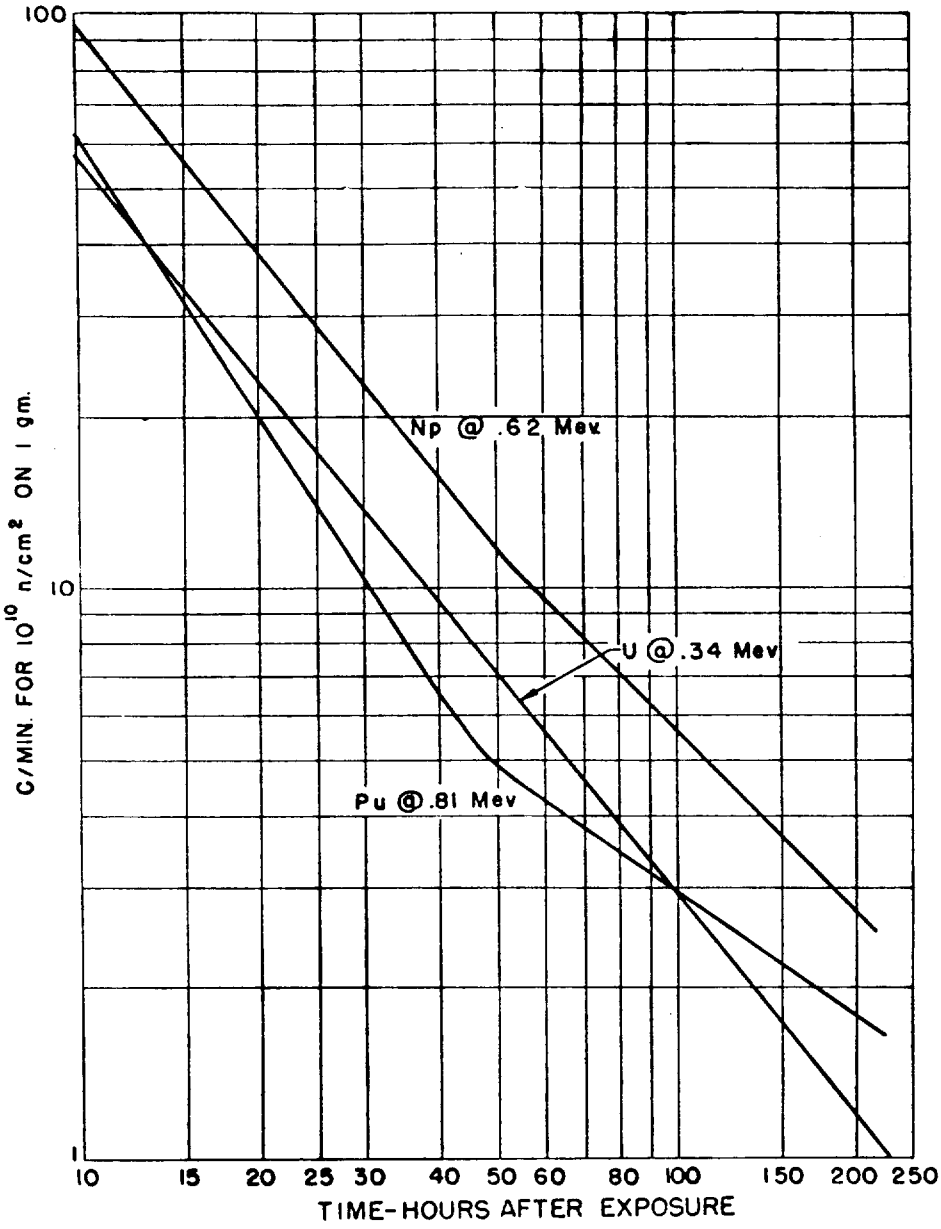

Fig. 4.4 Calibration Curves

being detected and thus the statistical process responsible for the power law decay breaks down. A preliminary analysis incidates that the observed deviation is caused by the 0.83 Mev gamma ray from 1.68 day La^{140} growing in from 12.8 day Ba^{140}. Additional work will be necessary to substantiate this and to choose a new set of optimum operating biases at very long times after exposure.

4.7 STANDARDIZATION

Due to drifts in the high voltage supply, amplifier gain, etc., the counting system must be standardized frequently. This is accomplished by using a standard gamma ray source and adjusting a fine control on the high voltage to reproduce a standard counting rate. The present system uses a half microcurie source of Co^{60}, in a standard lucite holder placed on the lead cap over the crystal, to give 35,000 c/min at the Pu bias of PHS 45 (0.81) Mev. The fine control is a 100 K, 10 turn, helipot in series with the high voltage lead to the 3 meg photomultiplier bleeder. One-tenth turn on the helipot changes the counting rate by 100 c/min under these conditions.

When it is necessary to calibrate another crystal-photomultiplier-amplifier setup, this can be accomplished by using this same Co^{60} source. The discriminator on the equipment being calibrated is set to have the same PHS versus gamma ray energy relation as the original equipment by adjusting the photomultiplier high voltage or the amplifier gain so that the photoelectric peaks of the Co^{60} lines or the high energy cutoff of the integral spectrum occur at the same PHS settings on both sets of equipment. The geometry and sensitivity factors are then determined by counting the standard source at the standard biases for Pu, Np, and U. A Cs^{137} source can be used conveniently to provide a check on the new calibration.

4.8 MINIMUM DETECTABLE NEUTRON INTENSITY

It is assumed that for field conditions one would be satisfied with counting a minimum induced activity in a sample equal to 20 per cent of the sample background activity. An accuracy of 10 per cent of the induced activity is possible in a counting time of 5 to 10 minutes due to the high sample background. The number of neutrons per cm^2 necessary to give this counting rate has been calculated from the calibration curves and the background data (Figs. 4.3 and 4.4) and is shown in Fig. 4.5. The calculations have been made for the following cases - 1.0 gm Pu, total background - 350 c/min; 0.1 gm Np, total background - 500 c/min; and 0.66 gm U, total background - 520 c/min.

4.9 NEPTUNIUM ACTIVATION ANALYSIS

Analysis of the UPSHOT-KNOTHOLE results[44] and of unpublished work at the ORNL 86 in. cyclotron showed that Np exposed in the standard B_4C holders and counted under the same conditions as Pu did not follow the standard fission product decay observed in Pu. Instead, the results could be interpreted in terms of the fission process plus the formation of Np^{238} by neutron capture, with subsequent beta decay with a 50 hr half life and the emission of a one Mev gamma ray. When

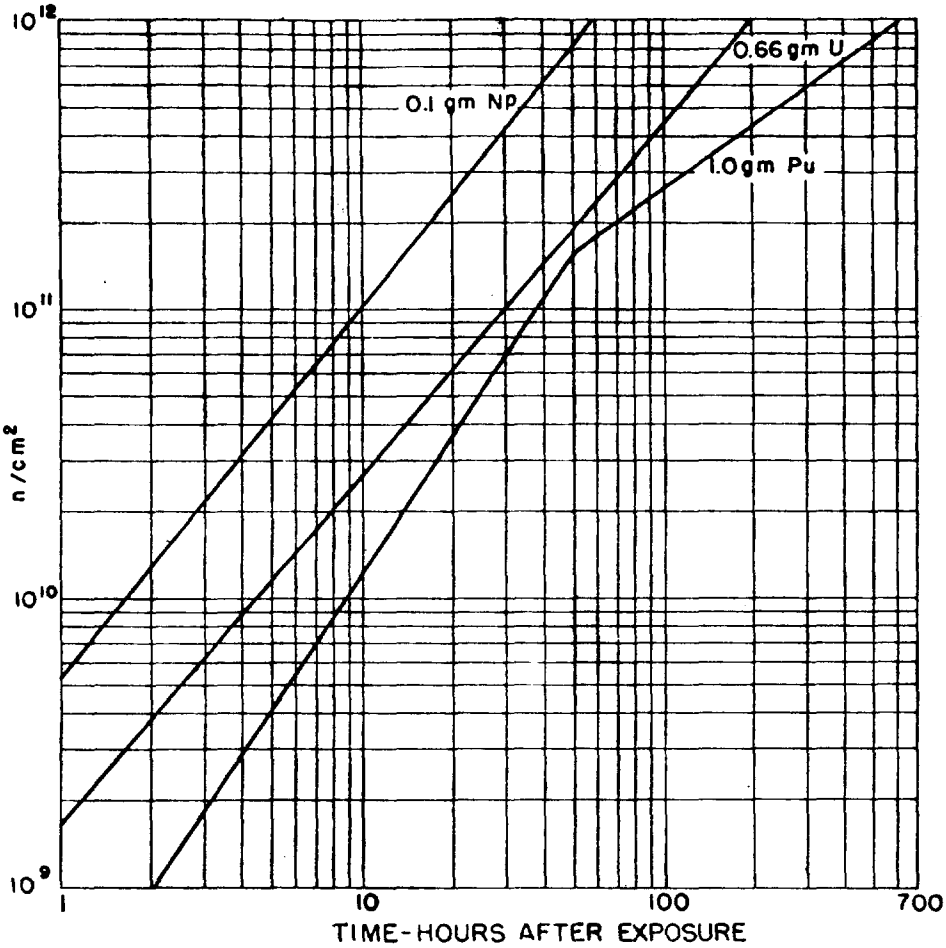

Fig. 4.5 Minimum Detectable Neutron Intensity

counting within a few hours of exposure is possible, the results can be analyzed in terms of a composite decay curve and the counting rate due to the fission product gamma rays determined. Since very early recovery is not always possible, an attempt was made to eliminate as much as possible of the neutron capture reaction. Np^{237} has a thermal neutron capture cross section of 170 barns and the assumption was made that it also has a fairly high capture cross section in the epithermal region. Preliminary tests at the cyclotron showed that additional boron shielding gave a resolvable decay curve at 25 hr. The Np holders used in the CASTLE tests contained 2.9 gm/cm^2 of pure metallic B^{10}, giving an attenuation of 1.1×10^{-7} at 50 and .006 at 500 ev, as compared to .015 and 0.26 for the 5.5 gm/cm^2 of normal B_4C in the standard Pu-U holders. As a further safety factor against thermal neutron activation the samples were shielded with 0.020 in. of cadmium.

Unfortunately, the two Np samples available were not recoverable after the second shot at CASTLE, though the recovery of some of the Pu and U samples at 120 hr after exposure showed that this would have been an excellent test of the analysis given above. It also showed that the observed fission product decay rates of Pu and U exposed to fast neutrons were the same for at least 250 hr after exposure as for Pu exposed to thermal neutrons.

4.10 RESULTS

The results obtained for the first two shots at CASTLE are shown in Table 4.1. The large amount of fallout and consequent operational and transportation difficulties resulted in a delay of five days between exposure and the start of counting. The activity of the samples was followed for another four or five days to establish that they decayed at the rate observed in the laboratory with thermal neutron activation of Pu. The counting rates at 200 hr were of the order of 10,000 c/min for the Pu samples and 500 c/min for the U samples.

TABLE 4.1 - Fission Detector Data

Shot No.	Range (ft)	$n/cm^2 \times 10^{-12}$		Pu/U
		Pu Flux	U Flux	
1	6000	150	5.3	28
	6000	190	6.5	29
	7775	Station damaged		
2	5100*	52	5.4	9.6
	5400*	Station damaged		
	5700	Station damaged		
	6000	31	2.1	15

*Np installed at these two stations was not recoverable.

The higher flux measured at a greater distance from ground zero on the first shot has not been satisfactorily explained. The inversion in the U flux shows that thermal neutron effects (i.e., a "leak" in one of the B_4 (holders) could not have been responsible. The only reasonable possibility seems to be that some ground structure partially shielded the closer station, although care was taken to avoid this on the installation of the stations.

PART III

EXPERIMENTAL GERMANIUM FAST NEUTRON DOSIMETERS

CHAPTER 5

EXPERIMENT DESIGN

5.1 BACKGROUND AND THEORY

The intial exploration of this method of measuring fast neutron energy flux was undertaken on a small scale as Project 29.2 of the Civil Effects Test Group in UPSHOT-KNOTHOLE. The results were encouraging enough to indicate that attempts should be made to refine the method to obtain higher sensitivity and reliability.

The Naval Research Laboratory became interested in setting up some germanium dosimeters at CASTLE. University of California, Los Angeles agreed to supply Project 2.3 with improved dosimeters for 15 stations. A new supply of single crystal germanium was purchased from Hughes Aircraft Co., and was specially prepared by Dr. M. Becker to provide optimum properties and purity for the intended application.

Fast neutrons produce Ge atom recoils in the crystal lattice. These recoils produce defects in the lattice structure which trap electrons coming from the Fermi levels. The unoccupied Fermi levels or "holes" act as if they were positive electrons endowing the crystal with conductivity. Hence a decrease in resistance represents the effects of the fast neutron flux to which the samples were exposed. The magnitude of the effect as a function of neutron energy has not been studied. Since dislocation is the effect measured, any neutron transferring sufficient energy can produce the effect. In this work it is

assumed that the cross section for a dislocation is the geometrical collision cross section. A low measuring temperature is used to avoid the shunting effect of electrons appearing in the conduction band by thermally excited transitions.

5.2 EXPERIMENTAL PROCEDURE

The new germanium strips were the same thickness (about 0.030 in.) as those used previously, but they were 2 mm wide and 4 mm long, instead of about 3 mm wide and 10 to 15 mm long. Instead of soldering on copper strip leads, the butt ends of the strips were tinned with ordinary solder. For measurement of the electrical resistance at low temperature, 10 strips were held in a specially constructed holder (Fig. 5.1). The small crystals were held in slits in a micarta strip. The tinned ends of the crystals made common electrical contact on one end with a metal sheet, and on the other end were contacted by individual phosphor bronze springs. The terminal on each spring was connected by an insulated wire to the measuring instruments.

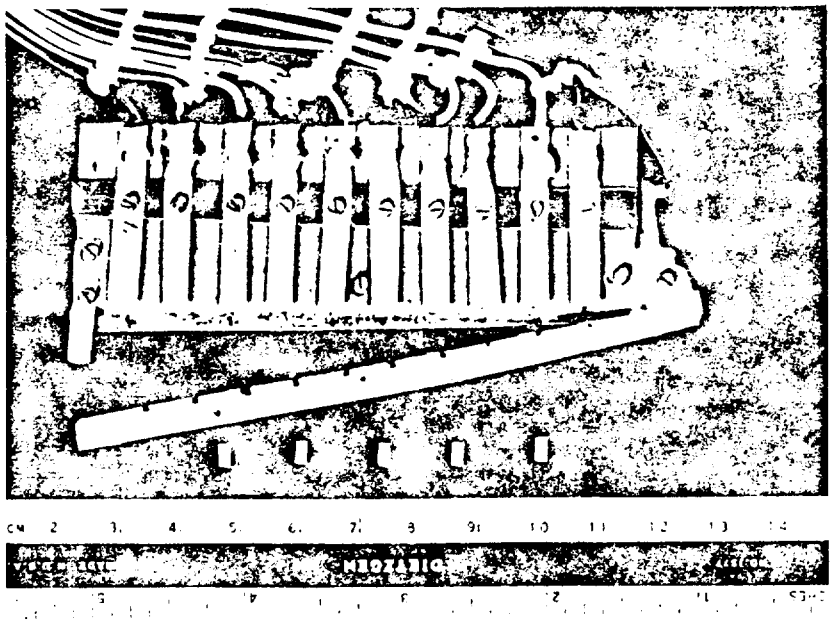

Fig. 5.1 Special Holder for Measurement of Germanium Strips

The whole assembly after being loaded was lowered into a wide-mouth Dewar flask containing a very low viscosity silicone liquid. The temperature of the bath was kept at -30°C by adding dry ice to the

bath as needed. The resistances of the strips were accurately measured and recorded.

The measured strips were placed in a multiple pocketed sack of shaved teflon. Teflon was used to avoid contact of the germanium with hydrogen containing material that might produce recoil protons that would penetrate slightly into the germanium. The teflon sack was packed in fiber glass in a slot in a steel bar, as shown in Fig. 5.2. After the cover was screwed in placed on this unit, it was then ready to be mounted on the Project 2.3 instrument line in the field.

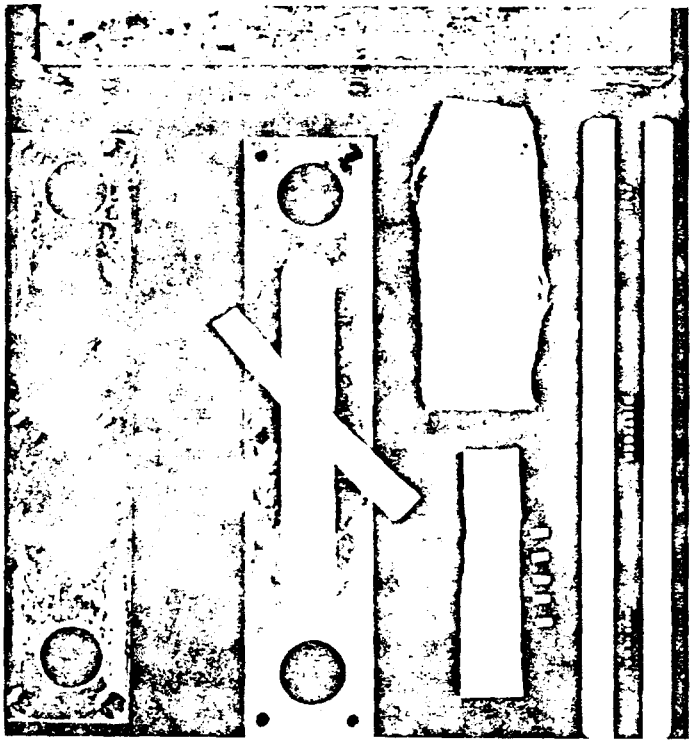

Fig. 5.2 Method of Packing of Germanium Strips in Field Test Container

Upon receipt of the samples after field exposure, they were remeasured at -30°C. The decrease in resistance, represents an effect of the fast neutron flux to which they were exposed.

5.3 CALIBRATION

Two calibration runs were made at the Crocker Lab. (UCLA) on the cyclotron using the Be (dn) reaction. The exposures were made at two

distances from the target. The results of these calibration runs are tabulated below. The great spread in the result is to be noted, it is felt that this error may be due, in part at least, to the method of attaching the leads to the germanium crystals and to the overall sample design. Recent improvements in sample preparation are aimed at correcting this difficulty.

TABLE 5.1 - Germanium Calibration Data

Distances	Flux	Change in Cond. (mho)	Calib. neuts/mho
5 in.	7.27×10^{12}	$205 \times 10^{-4} \pm 23$	3.7×10^{14}
10 in.	1.82×10^{12}	$123 \times 10^{-4} \pm 71$	1.5×10^{14}

It is assumed that the total cross section of germanium for fast neutrons remains approximately constant with increasing energy, so that for the calibration runs, which were made with neutrons between 15 and 20 Mev, the calibration is arrived at directly from the above figures. This number, an average from the calibration data is:

$$2.5 \times 10^{14} \text{ neuts/mho} \pm 50\%.$$

5.4 CALCULATIONS

The method of calculation of the change in conductivity is given below, where A is the change in conductivity:

$$A = 27.5 \left(\frac{1}{R} - \frac{1}{R_o} \right) \frac{L}{Wt}$$

R_o resistance (OHM) of crystal before exposure
R resistance (OHM) of crystal after exposure
L measured length (MM)
W measured width (MM)
t measured thickness (thousands of an inch)

The flux is then calculated by simply multiplying A times the calibration number.

$$\text{Flux} = 2.5 \times 10^{14} \text{ neuts/mho} \times A$$

5.5 RESULTS

Figure 5.3 is a graphical presentation of the results from Shots 1 and 2 on which germanium was exposed. The data are presented in the

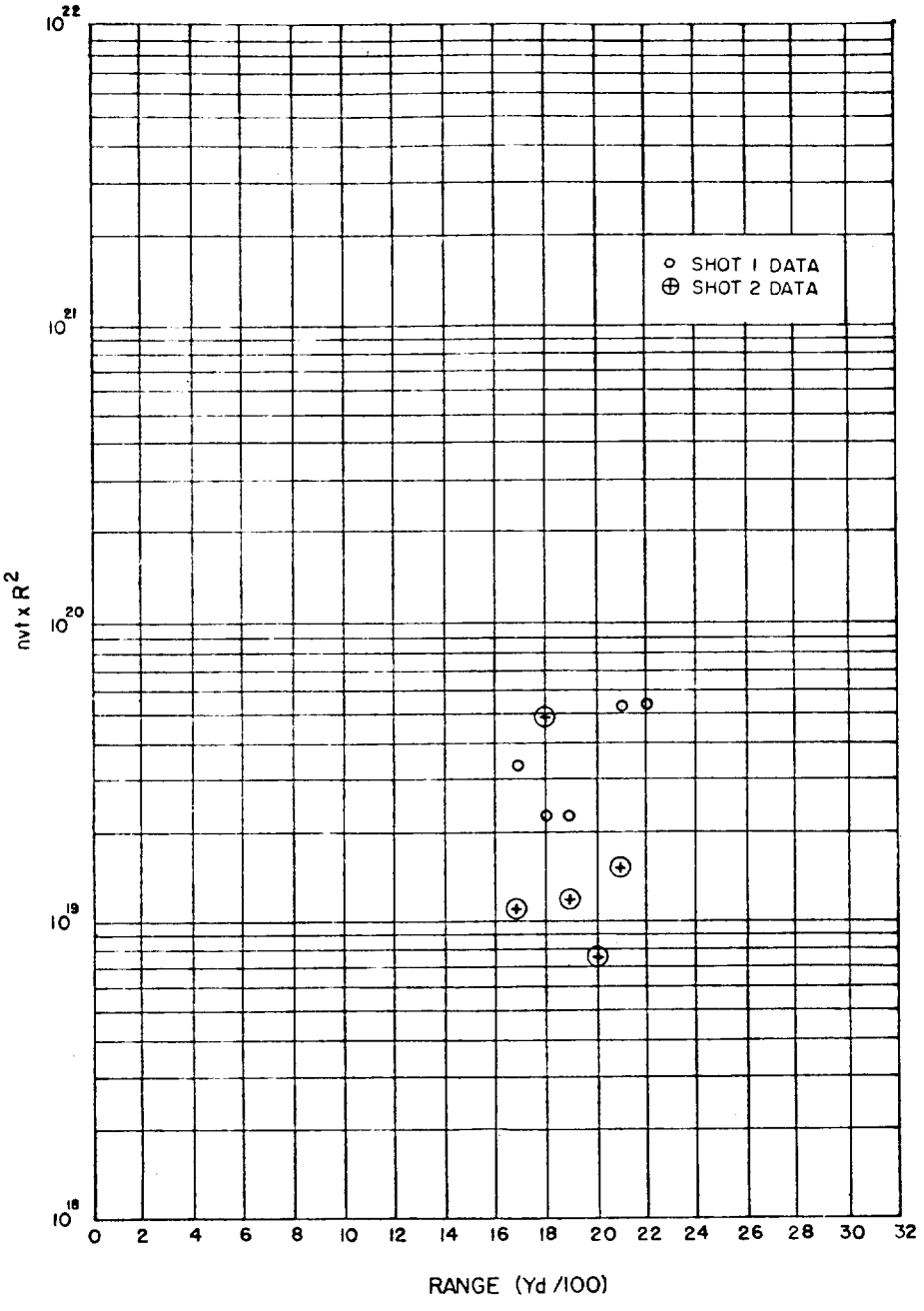

Fig. 5.3 Germanium Data

customary form of nvt x R^2 vs. Range. This was done mainly for the sake of uniformity in the report, for on examining the data it can be seen that it is quite difficult to characterize the data in the usual manner by quoting an e-fold distance and a range 0 intercept. The scatter in the points is quite large and data from both shots show a disconcerting rise in measured flux beyond 3000 yd. It has not been determined whether this is a coincidence in scatter or a function of the experiment. One thing is obvious that a more extensive line would have been advantageous, for it would have provided additional data which might have shown a trend at least.

TABLE 5.2 - Germanium Data

Shot	Range (yd)	ΔK Change in Cond. (mho)	nvt	nvt x R^2
1	1700	460.5×10^{-4}	1.2×10^{13}	3.4×10^{19}
	1800	287.9×10^{-4}	7.2×10^{12}	2.3×10^{19}
	1900	261.2×10^{-4}	6.6×10^{12}	2.4×10^{19}
	2100	460.8×10^{-4}	1.2×10^{13}	5.2×10^{19}
	2200	446.0×10^{-4}	1.1×10^{13}	5.2×10^{19}
2	1700	156.8×10^{-4}	3.9×10^{12}	1.1×10^{19}
	1800	623.5×10^{-4}	1.5×10^{13}	5.0×10^{19}
	1900	141.5×10^{-4}	3.6×10^{12}	1.3×10^{19}
	2000	73.9×10^{-4}	1.9×10^{12}	$.74 \times 10^{19}$
	2100	151.7×10^{-4}	3.8×10^{12}	1.7×10^{19}

Table 5.2 lists the data, by range, for Shots 1 and 2. The figures in the ΔK column are the averages of readings from seven crystals making up each sample, and in many cases the average of reading from two samples mounted on each station. The data yield flux figures of approximately the right order of magnitude; this at least is encouraging.

APPENDIX A

ISOTROPY OF NEUTRON FLUXES

A.1 NUMBER FLUX ISOTROPY

Elastic scattering will be of primary importance in the collision of neutrons with O and N atoms. In elastic scattering, the mean cosine of the scattering angle in the laboratory system, averaged over neutron directions, is given by[36]

$$\cos_m(a_{k-1}, a_k) = \frac{2}{3A}, \qquad (A.1)$$

where A is the mass number of the target nucleus.

Now, the cosine of the angle between the original direction a_o, of a neutron and its direction after n elastic scatterings,is, after averaging over azimuthal directions ψ in each collision.[37]

$$\cos(a_o, a_n)_{\psi av} = \cos(a_o, a_1)\cos(a_1, a_2)\ldots\cos(a_{n-1}, a_n) \qquad (A.2)$$

Substituting Equation A.1 into Equation A.2 the mean cosine of the directions of the n- scattered group of neutrons is:

$$\cos_m(a_o, a_n) = \left(\frac{2}{3A}\right)^n \qquad (A.3)$$

For air, $A \cong 14$ and $\frac{2}{3A} = 0.048$. Since a distance of 2000 yd in air corresponds to about 17 mean-free-paths, most of the neutrons arriving at the detector stations have gone through many collisions. Consider a group of neutrons that has gone through 16 collisions. The mean cosine of the direction of this group would be about 8×10^{-22}. Thus, the corresponding angle would be very close to 90^o to the original direction (the vector from the source); i.e., it is indicated that the distribution of directions of neutrons of this n^{th} scattered group is such

that the average of their cosines with a vector from the source is close to zero. Obviously, an isotropic distribution would satisfy such a condition, and an assumption of isotropy seems the most reasonable to make from an intuitive consideration of the large number of statistical events involved and the fact that each of these events has a distribution not too different from isotropic in the first place. The latter statement is true even at energies where the nitrogen absorption resonance is involved[31] - at least for the purpose of the fast-fission detector measurements.

A.2 ENERGY FLUX ISOTROPY

Consider the energy loss for scattering at the angle of the average cosine. $\text{Cos}_m\phi = \frac{2}{3A} \approx 0$, and the mean scattering angle, $\bar{\phi}$, is close to 90°. Since the laboratory angle ϕ and the center of mass system angle θ are related by

$$\tan\phi = \frac{A \sin\theta}{1 + A\cos\theta} \tag{A.4}$$

and since tan $\bar{\phi}$ is large, cos θ $(\bar{\phi})$ $- \frac{1}{A} = -0.072$. Now, the fractional energy, E'/E, remaining after scattering in the center of mass sytem is given by:

$$\frac{E'}{E} = \frac{A^2 + 1 + 2A\cos\theta}{(A+1)^2} \tag{A.5}$$

Substituting cos θ = -0.072, and A = 14, the fractional energy loss of a neutron scattering at the mean angle $\bar{\phi}$ is 0.867. Therefore, a neutron scattering elastically 16 times at the mean angle $\bar{\phi}$ will retain $(0.867)^{16}$ = 0.1 of its original kinetic energy. Thus, it can be seen that a good fraction of the neutrons were scattered below threshold energies by the time they reached the detector stations, and it is necessary for solid angle considerations to know if the energy flux as well as the number flux is isotropic.

To argue qualitatively that the energy flux is isotropic, consider the possibility that after n-1 collisions a distribution of neutrons is isotropic in direction but that neutrons of energy $E < E_t$ (where E_t is the threshold energy of the detector) are strongly peaked in the backward direction and neutrons of $E > E_t$ are strongly peaked forward. After the n^{th} collision, neutrons of $E < E_t$ from the n-1 group will still form a large part of the distribution $<E_t$, but each energy level of these neutrons will have been scattered with only slight anisotropy. Thus, neutrons in the n-1 interval $E < E_t$ will have become more closely isotropic in the n^{th} distribution. Neutrons of $E > E_t$ in the

(n-1) group will lose energy fractions from 0.75 to 1 in colliding with nitrogen atoms. Thus, neutrons in the energy region just greater than E_t will contribute an additional fraction of neutrons to the $E < E_t$ interval of the n^{th} distribution; but these neutrons will have been contributed with nearly isotropic, and the same, angular distribution, since the angular distribution is independent of energy (being always isotropic in the C.M. system for elastic scattering). Therefore, neutrons in the particular energy interval $E < E_t$ become more isotropic from the $(n-1)^{th}$ distribution to the n^{th} distribution; similar effects hold for the interval $E > E_t$.

Thus, since scattering a distribution tends to make the neutrons within an energy interval more isotropic, an assumption of complete isotropy of neutrons at many mean-free-paths seems reasonable for solid angle considerations in the fission detector measurements. Of course, the arguments above may not be valid in measurements where lower-energy neutrons are important, since in the tenth-Mev region, cross-sections become stronger functions of energy.

Exact calculations[38] of angular distribution are too difficult and unwarranted for the purposes of these experiments.

APPENDIX B

ABSORPTION BY LEAD PLUG

B.1 MEAN ATTENUATION OF BEAM WITHIN CONE OF HALF-ANGLE θ_e

Assuming isotropic incidence of neutrons, the average attenuation of the beams within a cone half-angle θ_e (Fig. 3.2) is:

$$\left(\frac{I}{I_o}\right)_{avg.} = \frac{\int_{\phi=0}^{\phi=2\pi}\int_{\theta=0}^{\theta=\theta_e} e^{-\mu t}\sin\theta\, d\theta\, d\phi}{\int_{\phi=0}^{\phi=2\pi}\int_{\theta=0}^{\theta_e}\sin\theta\, d\theta\, d\phi}$$

$$= \frac{\int_{\theta=0}^{\theta=\theta_e} e^{-\frac{\mu T}{\cos\theta}}\sin\theta\, d\theta}{1-\cos\theta_e} \qquad (B.1)$$

where θ and ϕ are the spherical coordinates with respect to the axis through the detector chamber, t_θ is the path length through the lead absorber at angle θ, T is the thickness of the lead plug, and θ_e is the limiting angle of incidence as estimated from Fig. 3.2.

To evaluate the integral in Equation B.1, let $v = (1/\cos\theta)$, $dv = (1/\cos^2\theta)\cdot\sin\theta\, d\theta$, $a = -\mu T$. Then[39]

$$\int_0^{\theta_e} e^{-\mu T/\cos\theta}\sin\theta d\theta = \int_{v=1}^{v=\frac{1}{\cos\theta_e}} \frac{e^{av}}{v^2}dv = e^a - e^{a/\cos\theta_e}\cos\theta_e + \int_{v=1}^{v=1/\cos\theta_e}\frac{e^{av}}{v}dv \qquad (B.2)$$

To evaluate the last integral in equation B.2, let $v = \frac{t}{-a}$, $dv = \frac{dt}{-a}$. Then,

$$\int_{v=1}^{v=1/\cos\theta_e} \frac{e^{av}}{v}\,dv = \int_{t_1=-a}^{t_2=-a/\cos\theta_e} \frac{e^{-t}}{t}\,dt$$

$$= \int_{t_1}^{\infty} \frac{e^{-t}}{t}\,dt - \int_{t_2}^{\infty} \frac{e^{-t}}{t}\,dt$$

$$= \left[-Ei(-x)\right]_{x=t_1} - \left[-Ei(-x)\right]_{x=t_2} \qquad (B.3)$$

using the notation $-Ei(-x)$ from reference 40.

From Equations B.3, B.2 and B.1

$$\frac{I}{I_o}_{avg} = \frac{1}{1-\cos\theta_e}\left[e^{-\mu T} - e^{-\mu T/\cos\theta_e}\cos\theta_e - \mu T\left\{\left[-Ei(-x)\right]_{x=\mu\bar{T}} \left[-Ei(-x)\right]_{x=\frac{\mu T}{\cos\theta_e}}\right\}\right] \qquad (B.4)$$

Equation B. 4 is used together with the tables of reference 40 in Sec. 3.5.5 for calculating the lead plug absorption factors given in Table 3.7.

BIBLIOGRAPHY

1. Neutron Measurements of Operation Snapper, WT-524
2. Neutron Measurements at Operation Upshot-Knothole, WT-720
3. Neutron Measurements of Operation Ranger, LABJ-2095
4. Preliminary Report on Greenhouse Neutron Measurements, LABJ-2102
5. Preliminary report, Operation Ivy, WT-621, Vol II.
6. U. FANO, Nucleonics 11, No. 9 (Sept. 1953)
7. "The Transuranium Elements," Vol. II, Seaborg, Katz, Manning, McGraw-Hill Book Co. (1949)
8. Ibid Cohen and Hull, p. 1167; other unpublished methods
9. Ibid., p. 1203
10. Ibid., pp. 1319-1324
11. Ibid., p. 1204
12. "The Transuranium Elements," Vol. 1, McGraw-Hill Book Co. (1949)
13. Ibid., Paper 3.5
14. Ibid., p. 46
15. A. Brodsky, L. W. Fagg, and T. D. Hanscome, NRL report to be published
16. Letter, C. L. Pigott, Oak Ridge National Laboratory, To E. L. Earl, NRL (1953)
17. NBS Handbook of Nuclear Data
18. Stations of Project 14.1, W. Biggers
19. Kanner and Barschall, Phys. Rev. 57, 372 (1940)
20. "Nuclear Fission and Atomic Energy," W. E. Stephens, The Science Press (1948)
21. P. Demers, Can. Journ. Phys. 31, 78-96 (1953)
22. "Experimental Nuclear Physics," Vol. I, E. Segré, John Wiley and Sons, Inc. (1953)
23. Ibid., Eqn. 30a, p. 230
24. Ibid., p. 229
25. "Nuclear Physics I," D. H. Frisch, Academic Press (1950), p. 55
26. Ibid., J. Rotblatt, Chapt. 3